Hydrothermal synthesis of high surface area ZIF-8 with minimal use of TEA

Hydrothermal synthesis of high surface area ZIF-8 with minimal use of TEA

V. V. Butova, A. P. Budnyk, E. A. Bulanova, C. Lamberti and A. V. Soldatov

Solid State Sciences 69 (2017) 13-21

doi: 10.1016/j.solidstatesciences.2017.05.002

http://www.sciencedirect.com/science/article/pii/S1293255816310020?via%3Dihub#abs0015

Hydrothermal synthesis of high surface area ZIF-8 with minimal use of TEA

V. V. Butova*[a], A. P. Budnyk[a], E. A. Bulanova[a], C. Lamberti[a, b] and A. V. Soldatov[a]

[a] International research center "Smart Materials", Southern Federal University, 5 Zorge str., Rostov-on-Don, 344090, Russia.

[b] Department of Chemistry, NIS and CrisDi Interdepartmental Centers, INSTM Reference Center, University of Turin, Via P Giuria 7, I-10125, Turin, Italy
*E-mail: vbutova@sfedu.ru; Tel: (863)219-87-75

Keywords ZIF-8; MOF; triethylamine; aqueous synthesis; high SSA.

In this paper we present, for the first time, a simple hydrothermal recipe for the synthesis of ZIF-8 Metal-Organic Framework (MOF) with a large specific surface area (1340 m^2/g by BET). An important feature of the method is that the product forms in aqueous medium under standard hydrothermal conditions without DMF and great excess of linker with the use of TEA as structure directing agent. The ZIF-8 crystal phase of the product was confirmed by XRD; this technique has been also exploited to check the crystallinity and to follow the changes in the MOF structure induced by heating. TGA and temperature dependent XRD testify the high thermal stability of the material (470 °C in N_2 and at 400 °C in air). The IR spectral profile of the material provides a complete picture of vibrations assigned to the linker and the metal center. The systematic investigation of the products obtained by increasing the TEA amount in the reacting medium from 0 to 25.5 mol equivalent Zn^{2+}, allowed us to understand its role and to find 2.6 mol equivalent Zn^{2+} as the minimum amount needed to obtain a single phase ZIF-8 material with the high standard reported above. The stability of the material under severe basic conditions makes it a promising candidate in heterogeneous catalysis. The material has shown high capacity in I_2 uptake, making it interesting also for selective molecular adsorption.

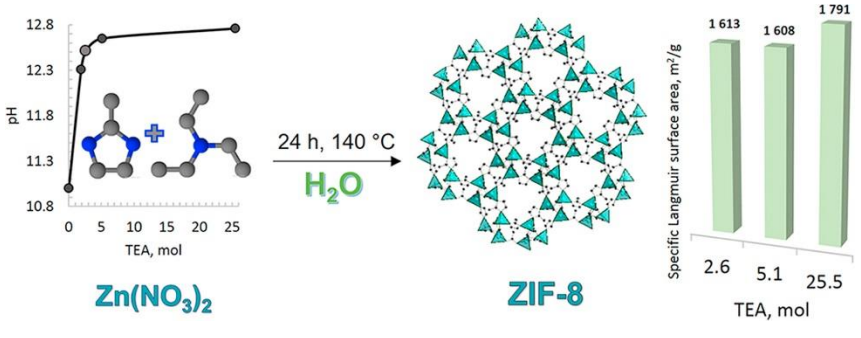

1. Introduction

MOFs are a rapidly expanding class of porous polymeric materials, that in about two decades of development has been reached more than 10000 entities and now possess clear principles of structural classification, rich and mature chemistry of synthesis, and sophisticated methods for experimental and theoretical analyses [1]. High specific surface area (SSA) and improved thermal stability of certain MOFs provide them performances comparable to that of inorganic adsorbents in the fields of gas separation/storage and catalysis [2-7]. However most of the synthesis and of the related tests are limited to the

laboratory scale and further progress towards industrial applications is generally hampered by some factors: (i) the high cost of MOFs production; (ii) the presence of remaining issues concerning chemical and mechanical stability under real conditions; (iii) issues in the synthesis reproducibility when dealing with scaled-up quantities [8]. Although, some types of MOFs are already available from commercial suppliers (in quantities up to kilos) [8-10], there is still a need for development of relatively simple, cost efficient and environmentally friendly way of synthesis of large amounts of MOFs.

The concept of reticular synthesis from molecular building blocks presented by Yaghi *et al.* [11] allowed for design and definition of MOFs sub-classes by the group of chosen metal for the node (or Secondary Building Unit) or the linker types. For the latter, the most studied are carboxylate and pyridyl based compounds, while the non-carboxylate ones are less frequently reviewed [12]. Studying divalent metal imidazolates, Huang *et al*. [13] found that addition of a methyl or ethyl substituent at the 2-position of the imidazolate ligand leads to formation of zeolite-type MOFs possessing exceptional chemical and thermal stability. In these materials, known as ZIF (Zeolitic Imidazolate Frameworks), a divalent metal atom (Zn, Co) is tetrahedrally surrounded by nitrogen atoms from the five-membered imidazole rings serving as a bridging linker, *i.e.* a link connecting the metal centres in the three-dimensional (3D) framework. By using 2-methylimidazole (Hmim) as a linker the MOF with general formula $[(Zn(mim)_2 \cdot 2H_2O)_\infty]$ was obtained. The structure has the regular zeolitic sodalite (SOD) topology and termed as ZIF-8 in a systematic work of Park *et al*. [14]. Summarizing the key factors for reproducible preparation of ZIFs are, according to Yaghi et al.: (i) linker functionalization; (ii) amide solvent medium (both playing the role of a structure-directing agent); (iii) control over the reaction conditions for crystal growth [14]. Zinc imidazolates were already tested for applications in gas separation [15-19], catalysis [20-22], gas sensing [23, 24], and even in radioactive iodine adsorption [25, 26]. Every application exploits certain properties of the MOF. Gas separation needs a highly porous material with tunable pore size [27] and ZIF-8 showed promising performance in the recovery of hydrogen from methane [17] or larger molecules [16], separation of ethane–propane, ethylene–propylene and ethylene–propane mixtures [28]. Instead, iodine adsorption requires open pores, high SSA, thermal and chemical stability of the adsorbent [26]. Catalytic applications expect material to be thermally stable because catalysis is normally performed under heating [6, 21], and to preserve stability under action of solvents for possible reuse [22].

In many potential applications, the large SSA of the MOF is the highly-deserved feature. Looking to develop a scalable and economically favorable synthesis route for production of ZIF-8 with high SSA, researchers faced noticeable difficulties. It has been established from the early reports on ZIFs, that synthesis in organic solvents like methanol or dimethylformamide (DMF) leads to a highly porous material. For example, Cravillon *et al.* [29] reports one of the highest values of the SSA obtained for ZIF-8, (1617 m^2/g BET, Brunauer–Emmett–Teller theory of adsorption). The samples were prepared in methanol within 24 h of reaction time with n-butylamine as a modulator. Nearly the same SSA (1630 m^2/g) was reached by Park *et al.* [14] who produced the MOF in DMF during 24 h. In our recent work [30] ZIF-8 with SSA of 1419 m^2/g was obtained in DMF in just 15 min by microwave-assisted heating.

The modern chemistry goes “greener”, looking to avoid (or, at least limit) both toxic and expensive solvents in conventional synthesis routes. An obvious alternative to organic solvents is water, however, the production of porous materials with high SSA in aqueous solutions is rather challenging [31].

In the literature, there are however a few ways to increase SSA of ZIF-8 water-based synthesis, as detailed in the Table S1 of the ESI. The first approach is to increase Zn to

Hmim ratio up to 1:40 and more. For example, in Jian *et al.* [32] the highest SSA (1126 m^2/g) was obtained using the Hmim : Zn molar ratio of 70. Kida *et al*. [33] achieved 1520 m^2/g starting from Zn : Hmim = 1 : 40. Pan *et al*. [18] adopted a room temperature (RT) synthesis with ratio Zn : Hmim = 1 : 70, which results in material of 1079 m^2/g. However, introducing a linker in great excess has several drawbacks, including the presence of unreacted ballast linker in the product. Even after washing some of its quantity remain in the MOF being stuck inside the pores. Summarizing, the surplus cost of unreacted linker, the need for additional washing (and thermal treatment) of the product and the unavoidable loss of SSA due to a fraction of trapped Hmim molecules, make industrial adoption of this synthetic approach economically unfavorable.

The second way is to adopt special synthesis routes. For example, Bao *et al*. [34] obtained ZIF-8 material in water with rather high SSA of 1075 m^2/g by microwave-assisted treatment. Shi *et al.* [35] tried a hydrothermal synthesis to receive ZIF-8 from zinc acetate and Hmim, but the obtained product was identified as a dense monoclinic phase. To overcame this problem, authors had to use the peculiar "steam-assisted convection method" obtaining a ZIF-8 phase having a high SSA of 1470 m^2/g [35]. Fan *et al*. [36] obtained ZIF-8 nanoparticles with high SSA (1360 m^2/g) by adding surfactants. Post-synthetic treatment in this case included redispersion in ethanol and refluxing for 24 h. All these complications could obstruct the scale-up of the method.

The third route is based on the addition of an alkali component (sodium formate or n-butylamine or polyamine) into reaction mixture with the scope to facilitate deprotonation of the linker and initiation of framework formation. The most commonly used agent is triethylamine (TEA). Unfortunately, it is a rather toxic and flammable reagent, but it can be removed from washing water by immobilization [37], photocatalytic degradation [38] and bacteria action [39]. Its use makes no need for loading of big excess of linker into reaction mixture as shown by Gross *et al.* [40], who achieved ZIF-8 phase using a RT synthesis in water. They traced the influence of molar ratio Zn^{2+} : linker : TEA on the SSA of ZIF-8 reaching the BET values of 528 and 811 m^2/g (for ratios of 1 : 4 : 4 and 1 : 16 : 16, respectively). Nordin *et al*. [41] obtained ZIF-8 crystals in water with different amounts of TEA (0.5-3.5 ml) at RT. In all cases the SSA of obtained material did not exceed 500 m^2/g (BET).

Hence, the synthesis in organic solvents results in highly porous materials, however the method is not very economical and could lead to environmental pollution. The choice of aqueous medium makes synthesis more "eco-friendly" but to obtain equivalently porous material one should use a great excess of linker, or alkali additives or non-standard synthetic routes. Reviewing the literature, we found a lack of studies concerning the use of alkali agent like TEA in a hydrothermal synthesis of ZIF MOFs at moderated temperatures of 100-120 °C. Here we report on the role of different amounts of TEA (Zn^{2+} : TEA in the 1.9-25.5 range) in hydrothermal synthesis of ZIF-8 at 120 °C. Due to its toxicity we performed a systematic study aimed in establishing the minimum amount of TEA needed to obtain ZIF-8 material with high SSA. The so synthesized materials have been fully characterized by powder XRD, BET, FTIR, TGA, and TEM.

2. Experimental

2.1 Synthesis

The starting materials zinc nitrate ($Zn(NO_3)_2 \cdot 6H_2O$, 99%), 2-methylimidazole (Hmim, $C_4H_6N_2$, 97%), and triethylamine (TEA, $(C_2H_5)_3N$, 99%) were produced by Alfa Aesar and were used without further purification. Ultra-pure water (18 MΩ·cm) was produced by SimplicityUV (Millipore) from distilled water. Berghof's laboratory stainless steel high

pressure reactor BR-200 (autoclave) with temperature controller BTC-3000 was employed for the synthesis. The autoclave was situated on a magnetic stirrer in a fume hood.
For the synthesis zinc nitrate, Hmim and water were taken in molar ratio 1 : 4 : 1240, respectively. Amount of TEA was varied from 1.9 to 25.5 mol in respect to Zn^{2+}, see Table 1. Typically, zinc nitrate (0.6663 g, 2.2400 mmol) and Hmim (0.7307 g, 8.900 mmol) were dissolved in 25 ml of water each. First, TEA (0.800 ml, 5.771 mmol) was added to Hmim solution (to facilitate further reaction with zinc salt) and then both solutions were poured into a Teflon liner. The mixture in autoclave was heated to 120 °C under stirring and held at this temperature for 24 h. After cooling down the white product was collected by centrifugation (7000 rpm, 15 min) and washed with 50 ml of water, then dried in vacuum at 80 °C for 12 h. The reaction yield of 79.6% was calculated by a thermogravimetric analysis (TGA). Note, that because a highly porous MOF contains an undefined quantity of guest molecules in pores, it is difficult to determine the exact yield of the final product just by measuring its weight.

Table 1. Quantification of the amount of TEA added to the reaction mixture for the whole set of samples and phase of the obtained product. UDCPh = unknown dense crystalline phase, see text for details.

Sample code	TEA/Zn^{2+} molar ratio	TEA/total molar ratio	TEA mmol	Phase [a]
S_0	0	0	0	UDCPh
S_1.9	1.9	0.0015	4.256	UDCPh
S_2.0 [b]	2.0	0.0016	4.479	ZIF-8/UDCPh
S_2.6	2.6	0.0021	5.771	ZIF-8
S_5.1	5.1	0.0041	11.423	ZIF-8
S_25.5	25.5	0.0205	57.113	ZIF-8

[a] The phase has been determined by XRD, see Section 3.1 and Fig. 1.
[b] As sample S_2.0 contains a mix of two phases, the data concerning its characterization are reported in the ESI only.

2.2. Characterization techniques

The crystallinity of the samples was evaluated by means of X-ray powder diffraction (XRD) system ARL X'TRA (Thermo Scientific) using CuKα radiation. Sequence of XRD patterns in situ collected under dynamic vacuum during heating up to 400 °C was performed in heating cell accessory (Anton Paar) for ARL X'TRA. Instead, samples were heated in muffle furnace in the air up to 200 or 400 °C, held at this temperature for 2 h, cooled down to RT before powder XRD data collection. The analysis of diffraction patterns (including indexing of reflections and calculation of unit cell parameter) was done in Jana2006 software [42]. The SSA (BET value) and porosity of the samples were determined from nitrogen adsorption/desorption isotherms at –196 °C obtained on Accelerated Surface Area and Porosimetry analyzer ASAP 2020 (Micromeritics). The sample was activated at 300 °C for 24 h under dynamic vacuum before the measurement. The type of isotherm was assigned based on IUPAC classification [43]. Transmission electron microscopy (TEM) was performed on FEI Tecnai G2 Spirit TWIN transmission electron microscope operated at an accelerating voltage of 80 kV. Sampling was done by ultrasound treatment with isopropanol for 30 minutes. Average particle size was calculated as an arithmetic mean of a set of 60-100 values. Thermogravimetric analysis (TGA) was performed on thermal gravimetric analyzer (Netzsch) with samples held in corundum pans in a continuous flow nitrogen

atmosphere or in the flux of air with heating rate of 10°/min. Fourier transform infrared (FTIR) spectra in Mid-IR region were recorded on Vertex 70 (Bruker) spectrometer with 2 cm^{-1} resolution. For the measurement "in transmittance" the sample was mixed with KBr in 1:200 weight ratio and pressed into a disc of 0.5 mm thick. The IR spectra "in reflectance" mode were collected on pure materials on A225/Q Platinum ATR (Attenuated Total Reflectance) accessory in Far-IR region.

3. Results and Discussion

3.1. Phase determination

The whole set of samples, obtained by hydrothermal synthesis with different amounts of TEA, see Table 1, was measured by powder XRD to examine the crystallinity and phase purity of the product. The diffraction patterns of the samples are shown in Fig. 1 together with that of Basolite Z1200 (BASF), a commercial analogue of ZIF-8. It is clear from Fig. 1 that XRD patterns of the samples S_2.6, S_5.1 and S_25.5 exhibit the same Bragg peaks of Basolite Z1200. This profile also matches with structural data for ZIF-8, reported by Park *et al*. [14]. Careful comparison of our experimental patterns with the reported data (see Fig. S1 in ESI) undoubtedly validates these samples as single-phase ZIF-8 material. The phase has been indexed in cubic symmetry and in the I-43m space group (217), with unit cell parameter a = 17.0078(8) Å (see Fig. S2 in ESI).

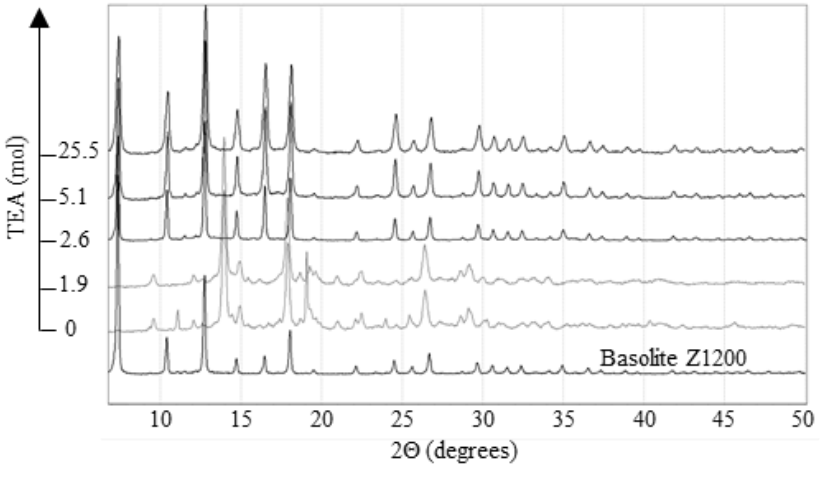

Fig. 1. XRD patterns of samples synthetized with TEA quantity of 1.9-25.5 mol (in respect to 1 mol of Zn^{2+}) and the pattern of Basolite Z1200 (BASF) measured for comparison.

Samples S_0 and S_1.9 exhibit the same unknown crystalline profile (gray curves in Fig. 1), clearly different from ZIF-8 SOD structure. It is worth to mention, that sample with 2.0 mol of TEA (S_2.0, not reported here for brevity) possess the same pattern with little inclusion from ZIF-8 phase, that is the only one present starting from sample S_2.6. A similar situation was already observed in several works [32, 34, 35, 41], where non-optimal synthesis conditions resulted in non-porous phases. In such cases, for failed synthesis, authors always found a crystalline dense phase. However only in the case of Bao et al. [34] the observed Bragg peaks correspond to those found here for S_0 and S_1.9 samples. Although the determination of this phase is behind the scope of the present work, samples S_0 and S_1.9 were subjected to all investigation techniques used to characterize the successful ZIF-8 synthesis. These studies are detailed in the ESI (Fig. S3, S4, S11 and S12) and are here just briefly summarized. BET analysis indicates that this phase corresponds to a dense material (SSA = 10.8 m^2/g). TEM study revealed the layered nature of this phase. The TGA of both S_0 and S_1.9 samples is very similar, showing a unique weight loss step of about 58 wt.%, starting

from 470 °C. (see Fig. S4 in ESI). Conversely to all other techniques (XRD, TEM, TGA, BET), showing completely different outputs for the ZIF-8 and the dense phase, the IR spectra of the two phases differs only by small details, discussed in section 3.4. This means that the local chemical groups are basically the same in both phases, just exhibiting a different long range ordering, that in one case results in pore formation and in the other not. Summarizing, in agreement with previous works [32, 41], we hypothesize that the formation of a dense and layered structure develops to the detriment of the ZIF-8 phase because an insufficient amount of TEA limits the deprotonation of the linker, see section 3.5 for a deeper discussion.

3.2. Thermal and chemical stability of the ZIF-8 phase

With the scope to provide a complete understanding of the thermal stability and guest mobility inherent for the obtained ZIF-8 material we combined study with TGA and XRD performed in the same conditions. This combination is extremally informative for MOFs characterization because TGA allows a quantitative determination of the mass leaving the sample, but it is blind to structural changes such as possible crystalline to amorphous phase transitions caused by pore collapse, that can however be detected by the XRD [44-47]. In this work, the studies have been duplicated to check the stability under both inert (N_2 or vacuum) and air atmospheres. The diffraction studies have been performed in situ (collecting the pattern in temperature along the heating ramp) and ex situ (collecting the pattern at RT after the thermal treatment at the desired temperature has been accomplished).

Fig. 2 reports TGA curves measured in air (black curve) and in nitrogen (gray curve) on sample S_2.6. TGA traces for samples obtained with higher TEA content show similar profile (see Fig. S6 in ESI). Both TGA traces in Fig. 2 have the typical shape for ZIF-8 MOF [13, 14, 28], while the difference in the two profiles reveals distinct thermal stability in the inert and oxidative media. More precisely, the first mass loss (marked "1" in Fig. 2), of 12.5 wt.%, occurs at about 310 °C and is attributed to the solvent evaporation from the material. It is followed by a slight decrement of 8.5 wt.% ("2" in Fig. 2) ending at 470 °C (in N_2) and at 400 °C (in air). This mass loss could be explained by the partial carbonization of organic residuals inside the pores of MOF. These temperatures may be taken as the limits of thermal stability of this ZIF-8 synthesis in different atmospheres. At the higher temperatures ("3" in Fig. 2) the linker decomposition occurs leading to the collapse of the MOF structure and explaining the most significant weight loss of 48.5 wt. %. The remaining 30.5 % of initial weight ("4" in Fig. 2) is due to formation of zinc oxide residual. Therefore, according to TGA data, the stoichiometric formula of ZIF-8 product is $Zn(mim)_{2.076}{\cdot}1.85H_2O$.

The top insets in Fig. 2 shows the diffraction patterns for S_2.6 sample activated at 200 °C (left) and 430 °C (right) and successively cooled down at RT (gray and black patterns refer to activations in vacuum and in air, respectively). The reported patterns confirm the picture emerging from TGA, stating that the stability of ZIF-8 is higher in vacuum. Under the air atmosphere (containing oxygen and moisture), the structure of MOF degrades faster, as it was already noticed in other works [28, 41, 47].

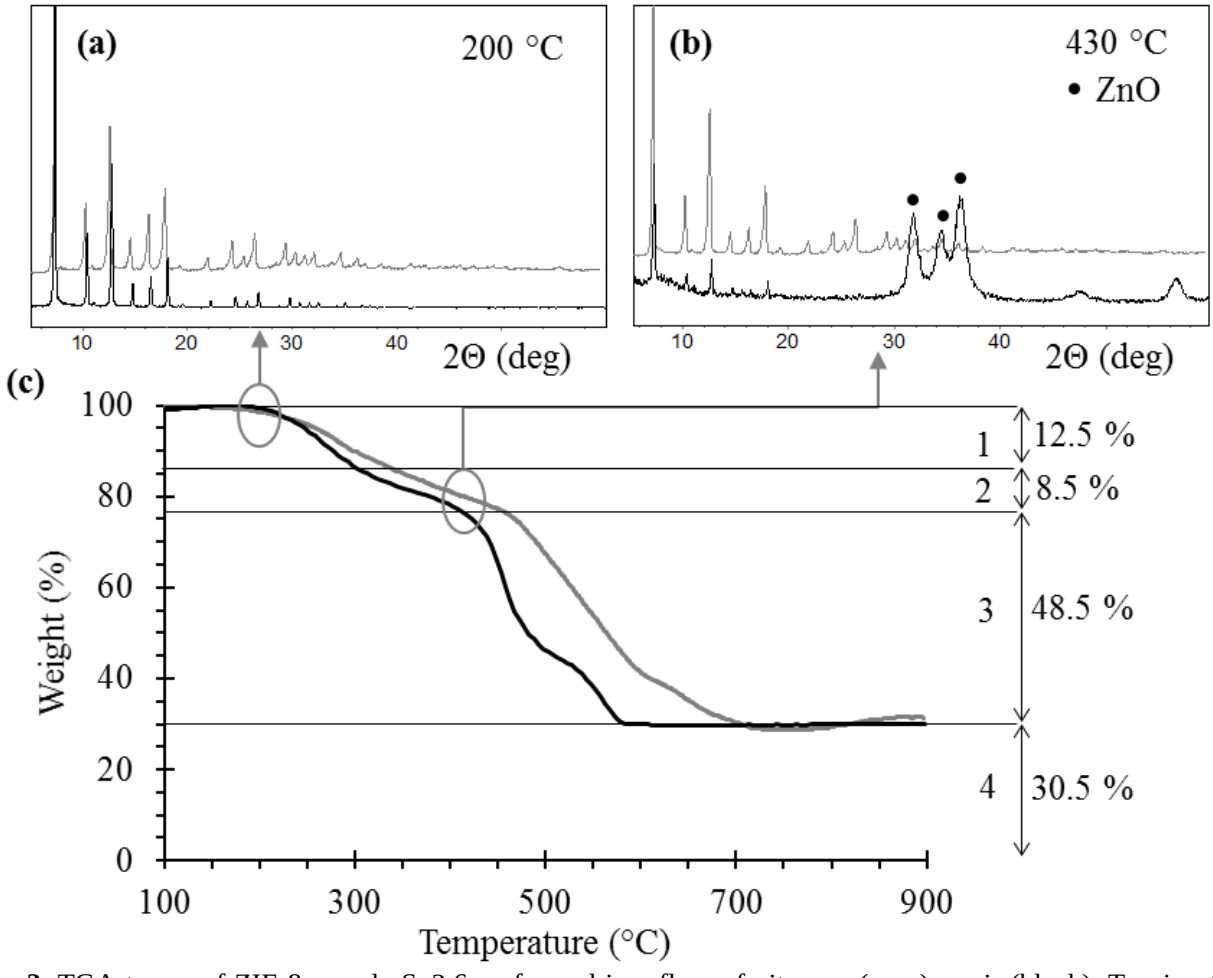

Fig. 2. TGA traces of ZIF-8 sample S_2.6 performed in a flow of nitrogen (gray) or air (black). Top insets reports the ex situ powder XRD profiles obtained at RT on sample S_2.6 activated at 200 and 430 °C (left and right sides, respectively). Gray and black patterns refer to the sample activated in vacuum or in air, respectively. Black circles mark ZnO reflections.

The thermal stability of the crystalline structure was also monitored by in situ X-ray thermo-diffractometry. Heating of ZIF-8 material under dynamic vacuum shows the stability of its phase up to 400 °C, see Fig. 3a. As expected, at higher temperatures the intensity of the high 2θ reflections decreases because of the increase of the thermal parameters [48], although a minor degradation of the crystalline quality at 400 °C cannot be ruled out. Curious is the shift of the Bragg peaks (Fig. 3b) and the consequent evolution of the lattice parameter *a* (Fig. 3c) along the activation process. First, *a* increases till 200 °C, then progressively decreases, at values even lower that that measured at RT. The fluctuation of the lattice parameter of a porous material along activation is quite common [49, 50] and is due to the fact that molecules adsorbed inside the pores (exiting the material along the activation) influence the *a* value even more strongly than the standard thermal expansion of physical nature.

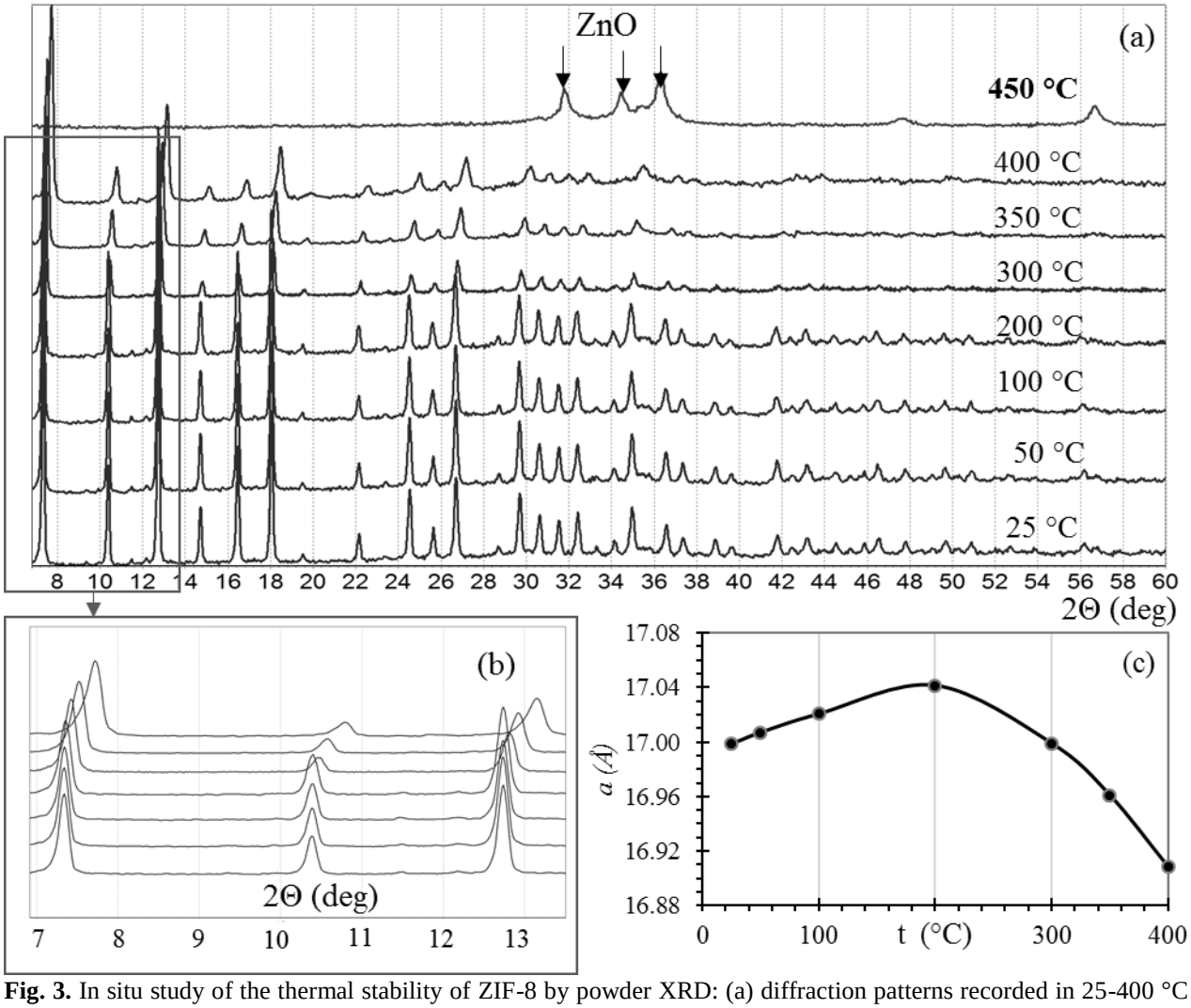

Fig. 3. In situ study of the thermal stability of ZIF-8 by powder XRD: (a) diffraction patterns recorded in 25-400 °C temperature range for sample S_2.6 under continuous removal of generated solvent vapor; sample at 450 °C was annealed in the air. (b) zoom of low 2θ reflections allowing to appreciate the shift and widening of the peaks upon heating; (c) Corresponding refined cell parameter.

Summarizing, the combination of TGA and XRD (both ex situ and in situ) data forms a complete picture of ZIF-8 thermal stability evidencing better resistance to elevated temperatures under inert atmosphere or in vacuum. This knowledge is relevant for designing possible application of the material. This combined study represents an improvement of the picture available in the literature. Indeed, Pan et al. reports XRD patterns on ZIF-8 activated at different temperatures and times in both air and vacuum, but reports TGA in He only [28]; Nordin et al. compares TGA in N_2 with XRD patterns for a sample heated in air at 300, 400, 500 and 600 °C [41]; He et al. provides TGA data in air up to 700 °C and XRD on one sample activated in air at 200, 250, 300 and 400 °C[47].

With the aim of verifying the stability of ZIF-8 for possible applications in catalysis and selective adsorption, we performed stability checks of the obtained material in water, acidic and basic solutions. Our XRD study confirms that after stirring for 24 h in water or 0.1 M solution of NaOH there was no changes in the ZIF-8 structure (see Fig. S5 in ESI). Conversely, the MOF was not stable in acidic medium (0.1 M HCl, see section 4 in ESI). We also performed adsorption tests for iodine uptake. We immersed the ZIF-8 sample in an ethanol iodine solution at RT. After

35 min of stirring the solution with ZIF-8 lost its colour and became transparent after centrifugation, while the control solution preserved its colour. The two solutions were additionally measured by UV-Vis spectroscopy, quantifying the observation (see Fig. S5 in ESI).

3.3. Morphological and volumetric study of the ZIF-8 phase

The effect of the TEA content on the average particle size and morphology of obtained ZIF-8 samples was determined by direct analysis of the TEM images. In all cases, well shaped rhombic dodecahedron crystals have been obtained (Fig. 4). Moving from sample S_2.6 up to sample S_25.5 the average particle size decreases by about on order of magnitude (Fig. 4 and Fig. S9 in ESI). This phenomenon was already observed previously [40, 41] and could be explained by the fact that high TEA content leads to high concentration of deprotonated linker molecules and fast reaction with zinc ions. Therefore, more nuclei forms in the reaction mixture resulting in smaller crystals.

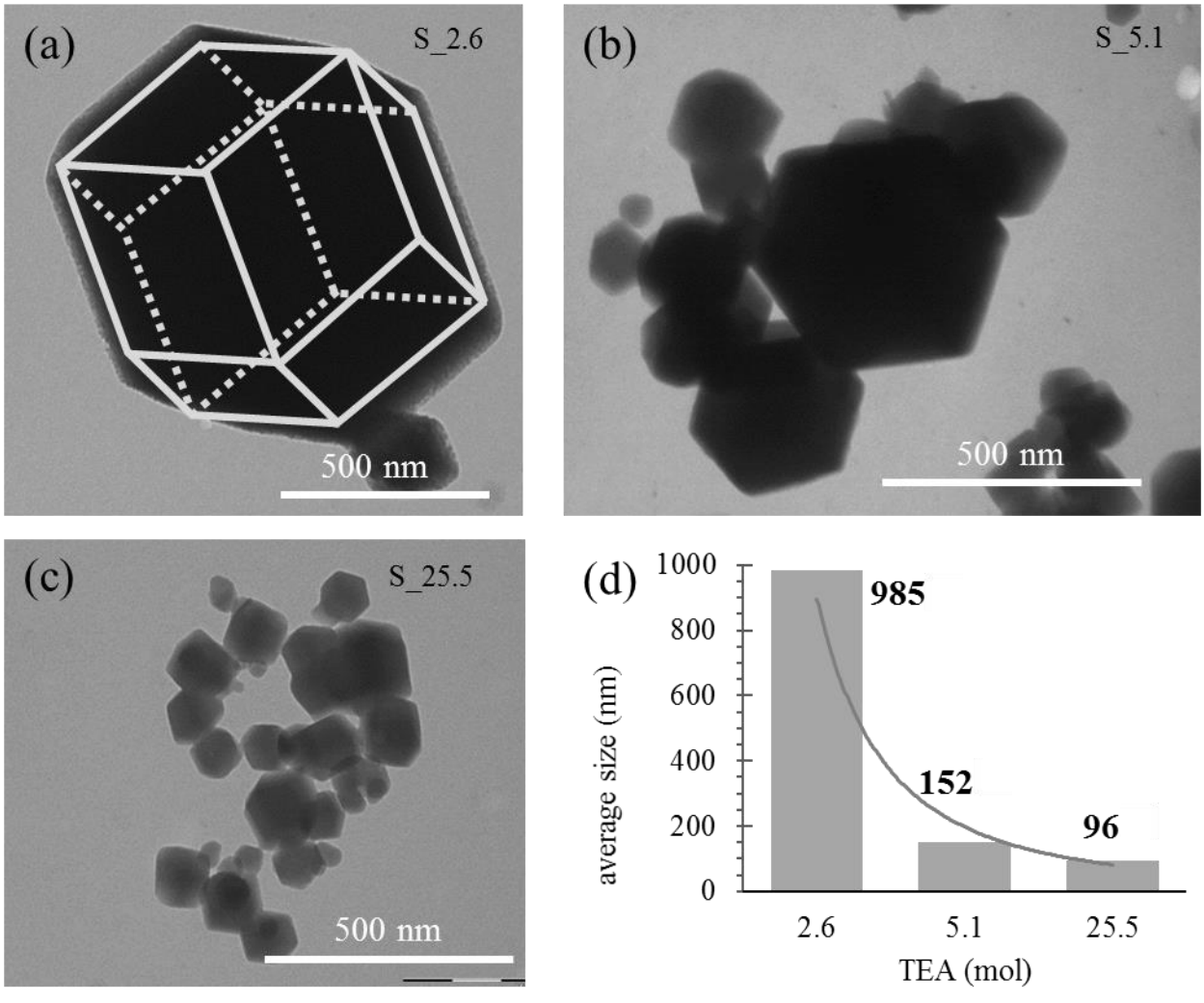

Fig. 4. Representative TEM images of ZIF-8 samples synthesized with different TEA content: (a) S_2.6; (b) S_5.1; (c) S_25.5. (d) average particle size of these samples. White polyhedron on the (a) section highlights the rhombic dodecahedron form of the crystal.

An important parameter allowing MOFs phases to be recognized is the SSA value of the material. Fig. 5 shows the adsorption/desorption isotherms of nitrogen at low temperature.

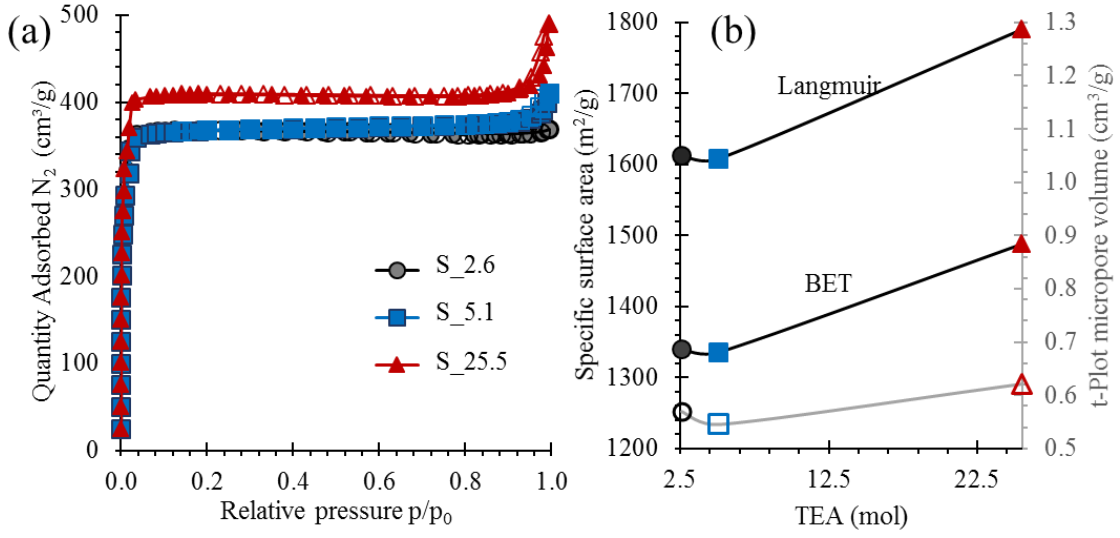

Fig. 5. (a) Isotherms of nitrogen physisorption at 77 K for ZIF-8 (samples S_2.6, S_5.1 and S_25.5). The adsorption branch is shown by filled markers and the desorption one by open markers. (b) left axis full symbols: SSA values calculated using BET and Langmuir models in respect to quantity of added TEA (calculated for 1 mol of Zn^{2+}). (b) right axis open symbols: as left for the pore volume.

The profile of the isotherms corresponds to that of type I, which is characteristic of microporous materials. For the ZIF-8 sample synthesized with the minimum amount of TEA, the SSA determined by the BET method gives 1340 m^2/g (1613 m^2/g by the Langmuir model); higher values are obtained for sample S_25.5. The obtained SSA are among the highest ones for ZIF-8 MOF obtained in the water media [28, 32, 41, 47]. Both SSA and pore volume follow the same trend along the series of samples (Fig. 5b). It is worth noticing that an increase of the TEA content by one order of magnitude (from sample S_2.6 to S_25.5) results in a moderate increase of the SSA (≈ 10%). Consequently, taking into account the toxicity of TEA, 2.6 mol equivalent Zn^{2+} are sufficient to obtain a high SSA ZIF-8 material. Further details about the measured N_2-adsorption isotherms are provided in Part 7 of ESI.

3.4. Vibrational study of the ZIF-8 phase and comparison with the dense phase

To control the molecular composition of the prepared samples, FTIR spectroscopy, widely used to characterize porous materials [51-53], was performed in the Mid-IR spectral region in transmission mode. The IR spectra collected on the whole series of synthesized materials (Table 1) are shown in Fig. 6. Independently on the long range structure of the products (ZIF-8 or unknown dense phase) the IR spectra appear quite similar at the first look and render those reported in the literature [14]. This means that the same chemical groups are present in both phases, although organized in a different way. Indeed, there is evident difference in some bands between two groups of spectra: samples S_25.5, S_5.1 and S_2.6 for the ZIF-8 phase and samples S_1.9 and S_0 for the dense phase. A full assignment of the absorption bands requires a parallel DFT study [45, 54, 55], that is beyond the scope of this paper. However, most of the observed bands are associated with vibrations of imidazole linker (see Fig. S8 in ESI). In particular, aromatic C–H stretching vibrations at 3135 cm^{-1}, C=N stretching vibration at 1584 cm^{-1} and ring vibrations in 1530-1350 cm^{-1} (breathing modes), 1350-800 cm^{-1} (bending in-plane vibrations), and below 800 cm^{-1} (out-of-plane

bending vibrations). A broad absorption band above 3000 cm^{-1} is caused by physisorbed water (which is normally present in the sample during the measurements in air).
The IR spectra of the ZIF-8 phase (samples S_25.5, S_5.1 and S_2.6 3-5), besides the bridging imidazolate signature (described above), contain a peculiar sequence of aliphatic C–H vibrations below 3000 cm^{-1}, which can be attributed to the spectral signature of entrapped TEA molecules. The shoulder at 1210 cm^{-1} was already assigned to the C–N stretch of TEA [40], supporting our attribution.
Instead, spectra of the dense phase (samples S_1.9 and S_0) do not contain spectral signs of TEA, evidencing its effective removal after washing owing to the absence of internal pores (see Fig. S4a in ESI). Conversely, there is a well-defined band at 3638 cm^{-1} due to the ν(O–H) stretching of nonbonded hydroxy group [45, 56, 57]. Also bands at 927 cm^{-1} and at 519 cm^{-1} are peculiar of the dense phase. The more accurate comparison between the IR spectra of the two phases is available in Fig. S11 in ESI, showing a zoom in the 1700-450 cm^{-1} region and stands for the different structural arrangement in materials obtained with low or high TEA content. The spectra in Far-IR region (see Fig. S12 in the ESI) allow to see the stretching and deformation vibrations of Zn–N, located at 421 and 329 cm^{-1}, respectively. The recorded spectra correspond to those known from the literature for ZIF-8, see for example the supporting information of ref. [58].

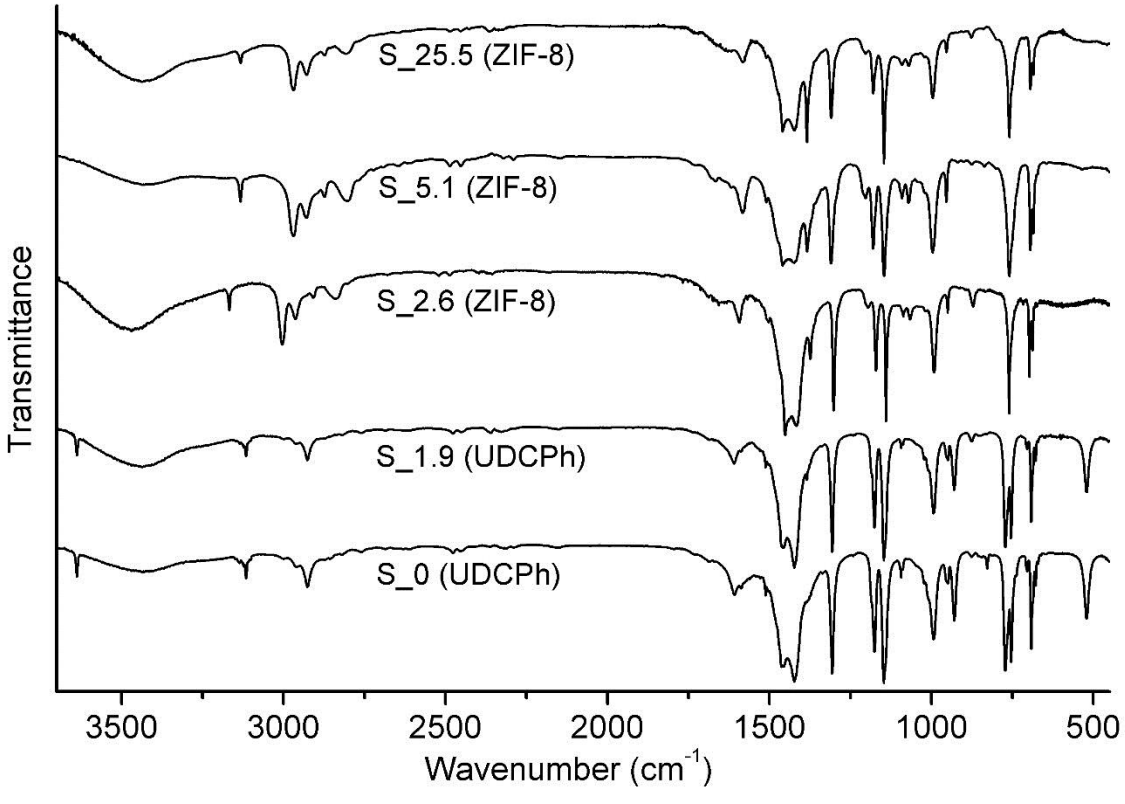

Fig. 6. FTIR spectra of ZIF-8 samples obtained with different TEA in transmittance. UDCPh = unknown dense crystalline phase.

3.5. Role of TEA in the ZIF-8 synthesis in aqueous medium
Based on the experimental observations discussed in sections 3.1-3.4, let us briefly discuss about the role of TEA in the mechanism of ZIF-8 crystal growth. Studying the growth of

ZIF-8 in methanol, McCarthy et al. [59] highlighted that, addition of alkaline agent (sodium formate) elevates the pH of the synthesis solution (from pH = 7.2 to pH = 8.3). This implies an increase of the quantity of deprotonated Hmim on the crystal surface, facilitating the interaction between ligands and Zn^{2+} ions with consequent improvement of the 3D intergrowth. Coming to synthesis performed in aqueous medium, Pan et al. [28] comment that, because water is less acidic than methanol, Hmim is getting deprotonated more easily in presence of water. Using a growth solution with Zn : Hmim = 1 : 70 ratio (pH ~ 9.5), they obtained the ZIF-8 phase without the need for addition of an alkaline solution. Kida *et al.* [33] reported several synthesis with the Zn : Hmim ratio 1 : x, with x ranging from 20 to 100. With a Zn : H_2O ratio fixed to 1 : 2228, they obtained the ZIF-8 phase only for $x \geq 40$. In all cases, they followed in time the evolution of the pH along the synthesis process, finding a final pH value of 9.0, 9.2, 9.5, 9.6 and 9.8 with x = 20, 40, 60, 80 and 100, respectively. All the here reviewed literature stress the important role of the pH value in the crystallization process of ZIF-8.

Coming to our synthesis, there is no doubt that at given ratio of Zn : Hmim = 1 : 4 the ZIF-8 phase could not be formed if no TEA (or too little amount) was added, see the whole discussion in sections 3.1-3.4 and in particular Fig. 1. In the following we will try to rationalize the role of the presence of TEA in the synthesis of ZIF-8 phase on a chemical ground. First, it is important underline that TEA must be added into the linker solution before introducing the metal salt. Otherwise, zinc ions will interact with HO^- groups, which are produced from the reaction of TEA with water, see Eq. (1). This will lead to a precipitation of $Zn(OH)_2$ and admixture of zinc oxide [36] in the final product after thermal treatment (see Section 10 in ESI).

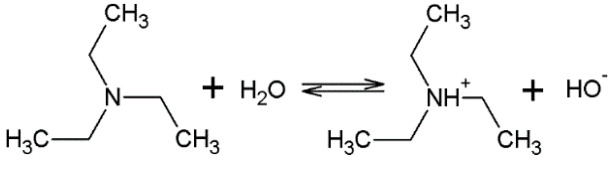

(1)

Second, Hmim is a Brønsted base and deprotonates some water molecules using its unshared electron pair as shown in Eq. (2). Thus, both nitrogen atoms of Hmim became protonated, leaving HO^- groups in the solution, which pH increases (measured pH = 11.0).

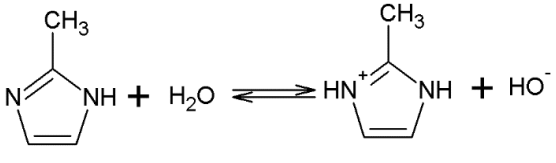

(2)

Protonated nitrogen atoms of Hmim cannot interact with zinc ions, blocking the synthesis of the ZIF-8 phase. On the other hand, TEA is a stronger Brønsted base in comparison to Hmim. Therefore, besides water deprotonation, Eq. (1), TEA addition to the linker solution leads also to the deprotonation of Hmim ligand, Eq. (3).

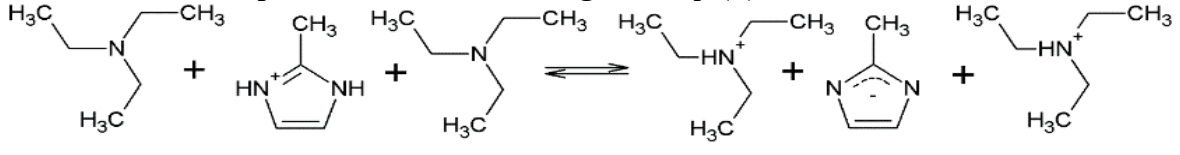

(3)

Eqs. (1)-(3) describe the three parallel processes occurring between Hmim and TEA in water solution. Their calculated equilibrium constants are $6.0 \cdot 10^{-4}$, $7.08 \cdot 10^{-7}$, and $4.0\ 10^{-2}$,

respectively (see Section 10 in ESI). Reactions in Eqs. (1) and (2) have basic HO^- groups as common product. The addition of alkali species in the growth medium [59] will shift the equilibrium of Eqs. (1) and (2) backwards to initial substances, what will lead to the decrease in concentration of protonated Hmim molecules and to the increase in that of deprotonated TEA. TEA and Hmim are in proton-transfer equilibrium according to Eq. (3) inducing a forward shift in equilibrium of reaction in Eq. (2) and a backward one in Eq. (1). Hence, all three reactions are interconnected and have a common equilibrium with a characteristic constant of $4.77 \cdot 10^{-5}$ (see Section 10 in ESI).

Summarizing, the synthesis parameters should be designed in order to displace the equilibrium of Eq. (3) to the right side because, once deprotonated, the Hmim linker is free to interact with the Zn^{2+} ions of the solution, see Eq. (4), and to start the reaction leading to the growth of the 3D structure of ZIF-8.

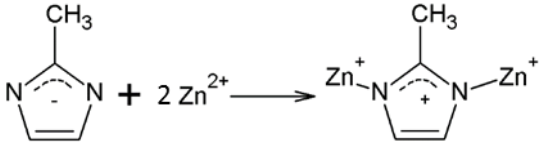

(4)

Obviously, an increase of the TEA content will shift the equilibrium of Eq. (3) in the desired direction. Now, it is important to establish the minimum concentration of TEA needed to have the sufficient amount of deprotonated Hmim ligand needed to run Eq. (4). According to the discussion of equilibria (1)-(3) the minimum TEA content can be determined measuring the pH of the synthesis solution as a function of the TEA content, as reported in Fig. 7 (blue data). It is clear from the plot that the pH value increases steeply at low TEA concentration, reaching a stable plateau after about 2 mol (Zn^{2+} equivalent). The pH value of about 12.5 defines the synthesis conditions leading to the formation of the ZIF-8 phase (black arrow in Fig. 7). Addition of an insufficient amount of TEA (less than 2 mol Zn^{2+} equivalent) results in a too low pH and the product is the UDCPh material (gray arrow in Fig. 7). This explains why, in the series of samples S_0, S_1.9, S_2.0, S_2.6, S_5.1 and S_25.5, the first sample exhibiting a fraction of ZIF-8 phase (together with UDCPh) is S_2.0, whose position in Fig. 7 is at the border of the plateau. The first pure ZIF-8 phase was obtained for sample S_2.6; consequently, the minimum amount of TEA needed to reach single-phase ZIF-8 is 2.6 mol Zn^{2+} equivalent.

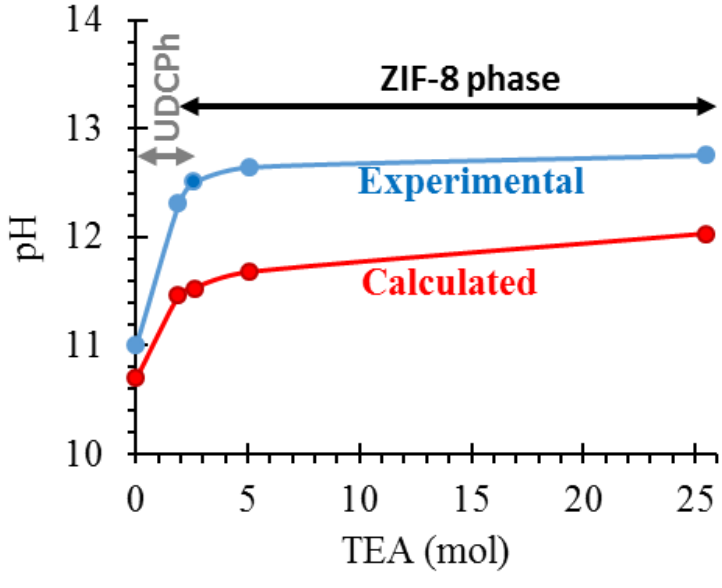

Fig. 7. Dependence of the pH of the reaction solution upon addition of increasing amount of TEA. TEA quantity is given in respect to 1 mol of Zn^{2+}. Blue line represents the measured pH values while the red one reports the calculated values, as described in Section 10 of the ESI. The appearance of a plateau in the pH value discriminates the synthesis conditions leading to the ZIF-8 structure (high TEA content, black arrow) from those resulting in the unknown dense crystalline phase (UDCPh, low TEA content, gray arrow).

Combining Eqs. (1)-(4) one obtains:

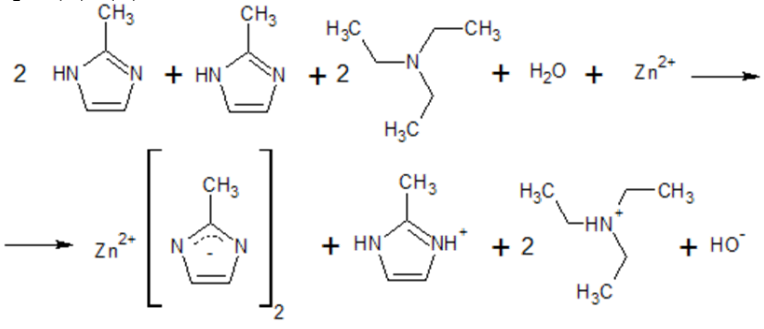

(5)

From which it emerges that one molecule of Hmim and two molecules of TEA are needed to deprotonate two molecules of linker in water medium. Therefore, the stoichiometric molar ratio of Hmim : TEA is 3 : 2. This ratio is in good agreement with our optimal ratio obtained from our study Hmim : TEA = 4 : 2.6, see Section 2.1, corresponding to Hmim : TEA = 3 : 1.95.

On the basis of the equilibrium constants of Eqs. (1)-(3), in the ESI we report the concertation of [HO^-] and of [H^+] formed in the reaction mixture after addition of different amounts of TEA, see Table S2 of ESI. The corresponding calculated pH values are shown in Fig. 7 as red curve. The calculated pH values well reproduce the trend observed in the experiment, particularly the plateau obtained for TEA concentration higher than 2 mol Zn^{2+} equivalent, but exhibit a systematic underestimation of the measured values, that can be ascribed by some inaccuracy of the adopted equilibrium constants.

Conclusions

In this work, we have reported the synthesis conditions to obtain a single-phase ZIF-8 material with high SSA (1340 m^2/g BET), high thermal stability (470 °C in N_2 and at 400 °C in air) in water (i.e. without organic solvents) with a low excess of Hmim linker (twice the stoichiometric value) with the assistance of TEA as structure directing agent. A series of 6 samples characterized a Zn^{2+} : TEA mol ratio ranging from 0 to 25.5 has been systematically investigated by temperature dependent XRD and TGA (both in inert and in air), N_2 sorption isotherms, TEM and FTIR techniques. From this set of experimental data we found that the minimum value of TEA needed to obtain a single phase ZIF-8 product is 2.6 mol equivalent Zn^{2+}. From a discussion on the reactions occurring in the synthesis ambient and from the measured pH values we rationalize the obtained minimum TEA value. This material represents an excellent candidate for applications in the fields of catalysis and selective molecular sorption due to its high SSA, high thermal stability, good resistance in strong basic environments and ability in adsorbing molecules of interest such as I_2.

Acknowledgements

This research is supported by the Mega-grant No.14.Y26.31.0001 of the Russian Federation Government.

Notes and references

[1] S. Kaskel, The chemistry of metal-organic frameworks: synthesis, characterization, and applications, Wiley-VCH, Weinheim, 2016.
[2] V.V. Butova, M.A. Soldatov, A.A. Guda, K.A. Lomachenko, C. Lamberti, Russ. Chem. Rev., 85 (2016) 280.
[3] J.L.C. Rowsell, O.M. Yaghi, Angew. Chem. Int.-Ed., 44 (2005) 4670.
[4] J.R. Li, R.J. Kuppler, H.C. Zhou, Chem. Soc. Rev., 38 (2009) 1477.
[5] L.J. Murray, M. Dinca, J.R. Long, Chem. Soc. Rev., 38 (2009) 1294.
[6] A. Corma, H. Garcia, F. Xamena, Chem. Rev., 110 (2010) 4606.
[7] J.R. Li, J. Sculley, H.C. Zhou, Chem. Rev., 112 (2012) 869.
[8] P. Silva, S.M.F. Vilela, J.P.C. Tome, F.A. Almeida Paz, Chem. Soc. Rev., 44 (2015) 6774.
[9] A.U. Czaja, N. Trukhan, U. Muller, Chem. Soc. Rev., 38 (2009) 1284.
[10] J.H. Cavka, S. Jakobsen, U. Olsbye, N. Guillou, C. Lamberti, S. Bordiga, K.P. Lillerud, J. Am. Chem. Soc., 130 (2008) 13850.
[11] O.M. Yaghi, M. O'Keeffe, N.W. Ockwig, H.K. Chae, M. Eddaoudi, J. Kim, Nature, 423 (2003) 705.
[12] S. Natarajan, P. Mahata, Current Opin. Solid State Mater. Sci., 13 (2009) 46.
[13] X.-C. Huang, Y.-Y. Lin, J.-P. Zhang, X.-M. Chen, Angew. Chem. Int.-Ed., 45 (2006) 1557.
[14] K.S. Park, Z. Ni, A.P. Côté, J.Y. Choi, R. Huang, F.J. Uribe-Romo, H.K. Chae, M. O'Keeffe, O.M. Yaghi, Proc. Nat. Acad. Sci. USA, 103 (2006) 10186.
[15] K. Li, D.H. Olson, J. Seidel, T.J. Emge, H. Gong, H. Zeng, J. Li, J. Am. Chem. Soc., 131 (2009) 10368.
[16] H. Bux, F. Liang, Y. Li, J. Cravillon, M. Wiebcke, J. Caro, J. Am. Chem. Soc., 131 (2009) 16000.
[17] Y. Liu, E. Hu, E.A. Khan, Z. Lai, J. Membrane Sci., 353 (2010) 36.
[18] Y. Pan, Z. Lai, Chemical Commun., 47 (2011) 10275.
[19] J. Yao, H. Wang, Chem. Soc. Rev., 43 (2014) 4470.
[20] H.-L. Jiang, B. Liu, T. Akita, M. Haruta, H. Sakurai, Q. Xu, J. Am. Chem. Soc., 131 (2009) 11302.
[21] C. Chizallet, S. Lazare, D. Bazer-Bachi, F. Bonnier, V. Lecocq, E. Soyer, A.-A. Quoineaud, N. Bats, J. Am. Chem. Soc., 132 (2010) 12365.
[22] U.P.N. Tran, K.K.A. Le, N.T.S. Phan, ACS Catal., 1 (2011) 120.
[23] G. Lu, J.T. Hupp, J. Am. Chem. Soc., 132 (2010) 7832.
[24] S. Liu, Z. Xiang, Z. Hu, X. Zheng, D. Cao, J. Mater. Chem., 21 (2011) 6649.
[25] N.R. Soelberg, T.G. Garn, M.R. Greenhalgh, J.D. Law, R. Jubin, D.M. Strachan, P.K. Thallapally, Sci. Technol. Nucl. Installat., 2013 (2013) Artr. n. 702496.
[26] J.T. Hughes, D.F. Sava, T.M. Nenoff, A. Navrotsky, J. Am. Chem. Soc., 135 (2013) 16256.
[27] B. Chen, F. Bai, Y. Zhu, Y. Xia, Micropor. Mesopor. Mater., 193 (2014) 7.
[28] Y. Pan, Y. Liu, G. Zeng, L. Zhao, Z. Lai, Chemical Commun., 47 (2011) 2071.
[29] J. Cravillon, R. Nayuk, S. Springer, A. Feldhoff, K. Huber, M. Wiebcke, Chem. Mater., 23 (2011) 2130.
[30] V.V. Butova, A.P. Budnik, E.A. Bulanova, A.V. Soldatov, Mendeleev Commun., 26 (2016) 43.
[31] E.L. Bustamante, J.L. Fernández, J.M. Zamaro, J. Colloid Interf. Sci., 424 (2014) 37.
[32] M. Jian, B. Liu, R. Liu, J. Qu, H. Wang, X. Zhang, RSC Adv., 5 (2015) 48433.
[33] K. Kida, M. Okita, K. Fujita, S. Tanaka, Y. Miyake, CrystEngComm, 15 (2013) 1794.
[34] Q. Bao, Y. Lou, T. Xing, J. Chen, Inorg. Chem. Commun., 37 (2013) 170.
[35] Q. Shi, Z. Chen, Z. Song, J. Li, J. Dong, Angew. Chem. Int.-Ed., 50 (2011) 672.
[36] X. Fan, W. Wang, W. Li, J. Zhou, B. Wang, J. Zheng, X. Li, ACS Appl. Mater. Interfac., 6 (2014) 14994.
[37] T. Cai, L. Chen, Q. Ren, S. Cai, J. Zhang, J. Hazard. Mater., 186 (2011) 59.
[38] A. Huang, L. Cao, J. Chen, F.-J. Spiess, S.L. Suib, T.N. Obee, S.O. Hay, J.D. Freihaut, J. Catal., 188 (1999) 40.
[39] C.-C. Wang, K.-L. Lu, X.-Y. Chen, Int. Biodeteriorat. Biodegrad., 59 (2007) 202.
[40] A.F. Gross, E. Sherman, J.J. Vajo, Dalton Trans., 41 (2012) 5458.
[41] N.A.H.M. Nordin, A.F. Ismail, A. Mustafa, P.S. Goh, D. Rana, T. Matsuura, RSC Adv., 4 (2014) 33292.
[42] V. Petricek, M. Dusek, L. Palatinus, Z. Kristall., 229 (2014) 345.
[43] K.S.W. Sing, D.H. Everett, R.A.W. Haul, L. Moscou, R.A. Pierotti, J. Rouquerol, T. Siemieniewska, Pure Appl. Chem., 57 (1985) 603.
[44] J. Hafizovic, M. Bjorgen, U. Olsbye, P.D.C. Dietzel, S. Bordiga, C. Prestipino, C. Lamberti, K.P. Lillerud, J. Am. Chem. Soc., 129 (2007) 3612.
[45] L. Valenzano, B. Civalleri, S. Chavan, S. Bordiga, M.H. Nilsen, S. Jakobsen, K.P. Lillerud, C. Lamberti, Chem. Mat., 23 (2011) 1700.
[46] G.C. Shearer, S. Chavan, J. Ethiraj, J.G. Vitillo, S. Svelle, U. Olsbye, C. Lamberti, S. Bordiga, K.P. Lillerud, Chem. Mat., 26 (2014) 4068.
[47] M. He, J. Yao, Q. Liu, K. Wang, F. Chen, H. Wang, Micropor. Mesopor. Mater., 184 (2014) 55.

[48] E. Borfecchia, D. Gianolio, G. Agostini, S. Bordiga, C. Lamberti, Characterization of MOFs. 2. Long and Local Range Order Structural Determination of MOFs by Combining EXAFS and Diffraction Techniques, in: F. Xamena, J. Gascon (Eds.) Metal Organic Frameworks as Heterogeneous Catalysts, Royal Soc Chemistry, Cambridge, 2013, pp. 143.
[49] M. Milanesio, G. Artioli, A.F. Gualtieri, L. Palin, C. Lamberti, J. Am. Chem. Soc., 125 (2003) 14549.
[50] G. Agostini, C. Lamberti, L. Palin, M. Milanesio, N. Danilina, B. Xu, M. Janousch, J.A. van Bokhoven, J. Am. Chem. Soc., 132 (2010) 667.
[51] C. Lamberti, A. Zecchina, E. Groppo, S. Bordiga, Chem. Soc. Rev., 39 (2010) 4951.
[52] F. Bonino, C. Lamberti, S. Chavan, J.G. Vitillo, S. Bordiga, Characterization of MOFs. 1. Combined Vibrational and Electronic Spectroscopies, in: F. Xamena, J. Gascon (Eds.) Metal Organic Frameworks as Heterogeneous Catalysts, Royal Soc Chemistry, Cambridge, 2013, pp. 76.
[53] S. Bordiga, C. Lamberti, F. Bonino, A. Travert, F. Thibault-Starzyk, Chem. Soc. Rev., 44 (2015) 7262.
[54] S. Chavan, J.G. Vitillo, D. Gianolio, O. Zavorotynska, B. Civalleri, S. Jakobsen, M.H. Nilsen, L. Valenzano, C. Lamberti, K.P. Lillerud, S. Bordiga, Phys. Chem. Chem. Phys., 14 (2012) 1614.
[55] L. Valenzano, J.G. Vitillo, S. Chavan, B. Civalleri, F. Bonino, S. Bordiga, C. Lamberti, Catal. Today, 182 (2012) 67.
[56] N. Masciocchi, S. Galli, V. Colombo, A. Maspero, G. Palmisano, B. Seyyedi, C. Lamberti, S. Bordiga, J. Am. Chem. Soc., 132 (2010) 7902.
[57] S. Chavan, J.G. Vitillo, D. Gianolio, O. Zavorotynska, B. Civalleri, S. Jakobsen, M.H. Nilsen, L. Valenzano, C. Lamberti, K.P. Lillerud, S. Bordiga, Phys. Chem. Chem. Phys., 14 (2012) 1614.
[58] Y. Hu, Z. Liu, J. Xu, Y. Huang, Y. Song, J. Am. Chem. Soc., 135 (2013) 9287.
[59] M.C. McCarthy, V. Varela-Guerrero, G.V. Barnett, H.-K. Jeong, Langmuir, 26 (2010) 14636.

Electronic Supplementary

Hydrothermal synthesis of high surface area ZIF-8 with a minimal use of TEA

V. V. Butova[*a], A. P. Budnyk[a], E. A. Bulanova[a], C. Lamberti[a,b] and A. V. Soldatov[a]

[a] *International research center "Smart Materials", Southern Federal University, 5 Zorge str., Rostov-on-Don, 344090, Russia*
[b]*Department of Chemistry, NIS and CrisDi Interdepartmental Centers, INSTM Reference Center, University of Turin Via P Giuria 7, I-10125 Turin, Italy*

Corresponding author: Vera V. Butova, butovav86@gmail.com

Content: page

1. Synthesis details and SSA of reported ZIF-8

N	*Metal : Linker : Solvent molar ratio*	*Eventual additives*	*Synthesis conditions*	*SSA (BET), m^2/g*	*Ref.*
1.	**Solvent: methanol**				
1.1	$Zn(OH)_2$: Hmim : MeOH =1 : 2 : 1229	NH_3OH	RT, 1 month	1030	[1]
1.2	$Zn(OH)_2$: Hmim : MeOH =1 : 2 : 63	NH_3OH	RT, 1 month	1460	[2]
1.3	$ZnCl_2$: Hmim : MeOH =1 : 1.5 : 250	HCOONa	100 °C, 4 h, MW	1496†	[3]
1.4	$Zn(NO_3)_2$: Hmim : MeOH = 1 : 4 : 500	Zn : n-$BuNH_2$ = 1 : 2-4	RT, 24 h	1617	[4]
2.	**Solvent: DMF**				
2.1	$Zn(NO_3)_2$: Hmim : DMF = 1 : 1 : 290	—	140 °C, 24 h, ST	1630	[5]
2.2	$Zn(NO_3)_2$: Hmim : DMF =1 : 1 : 290	—	140 °C, 24 h, ST	1413	[6]
2.3	$Zn(NO_3)_2$: Hmim : DMF = 1 : 1 : 266	—	140 °C, 24 h, ST	1705‡	[7]
2.4	$Zn(NO_3)_2$: Hmim : DMF =1 : 1 : 287	—	140 °C, 24 h, ST	1501‡	[8]
2.5	$Zn(NO_3)_2$: Hmim : DMF =1 : 2 : 165	—	120 °C, 24 h, ST	1560	[9]
2.6	$Zn(NO_3)_2$: Hmim : DMF =1 : 2 : 289	Zn:TEA = 1:3	140 °C, 15 min, MW	1419	[10]
3.	**Solvent: water**				
3.1	$Zn(NO_3)_2$: Hmim : H_2O = 1 : 70 : 1238	—	RT, 5 min	1079	[11]
3.2	$Zn(NO_3)_2$: Hmim : H_2O = 1 : 4-16 : 2254.7	Zn:TEA = 1 : 4-16	RT, 10 min	528-811	[12]
3.3	$Zn(NO_3)_2$: Hmim : H_2O = 1 : 40-100 : 2228	—	RT, 24h	1520-1600	[13]
3.4	$Zn(NO_3)_2$: Hmim : H_2O = 1 : 2 : 1444.9	Span 80, Tween 80	60 °C, 1h,	1360	[9]
3.5	$Zn(NO_3)_2$: Hmim : H_2O = 1 : 6 : 500	Zn:TEA = 1 : 0.5-3.8	RT, 30 min	418-492	[14]
3.6	$Zn(OAc)_2$: Hmim : H_2O =1 : 10 : 886	—	120 °C, 24h, water steam	1470	[15]
3.7	$Zn(OAc)_2$: Hmim : H_2O =1 : 10 : 1111	—	120 °C, 30 min, MW	1075	[16]
3.8	$Zn(OAc)_2$· : Hmim : H_2O =1 : 10-70 : 1280	—	RT, 24h	1126	[17]
3.9	$Zn(NO_3)_2$: Hmim : H_2O = 1 : 4 : 1240.2	Zn:TEA = 1:1.9 – 1:25.5	120 °C, 24h, ST	1329	This work

Remarks: †Argon; ‡ Langmuir surface area. Hmim – 2-methylimidazole, MeOH – methanol, DMF – dimethylformamide, $BuNH_2$ – n-Butylamine.

2. XRD profiles of as synthesized ZIF-8 sample

XRD patterns were measured on system ARL X'TRA (Thermo Scientific) using CuKα radiation. The generator setting was 40 kV and 40 mA, with a step size of 0.02° and a scanning rate 6° per minute. Profile analysis was done in Jana2006 program package considering cubic structure symmetry for space group of I-43m with four formula units per unit cell.

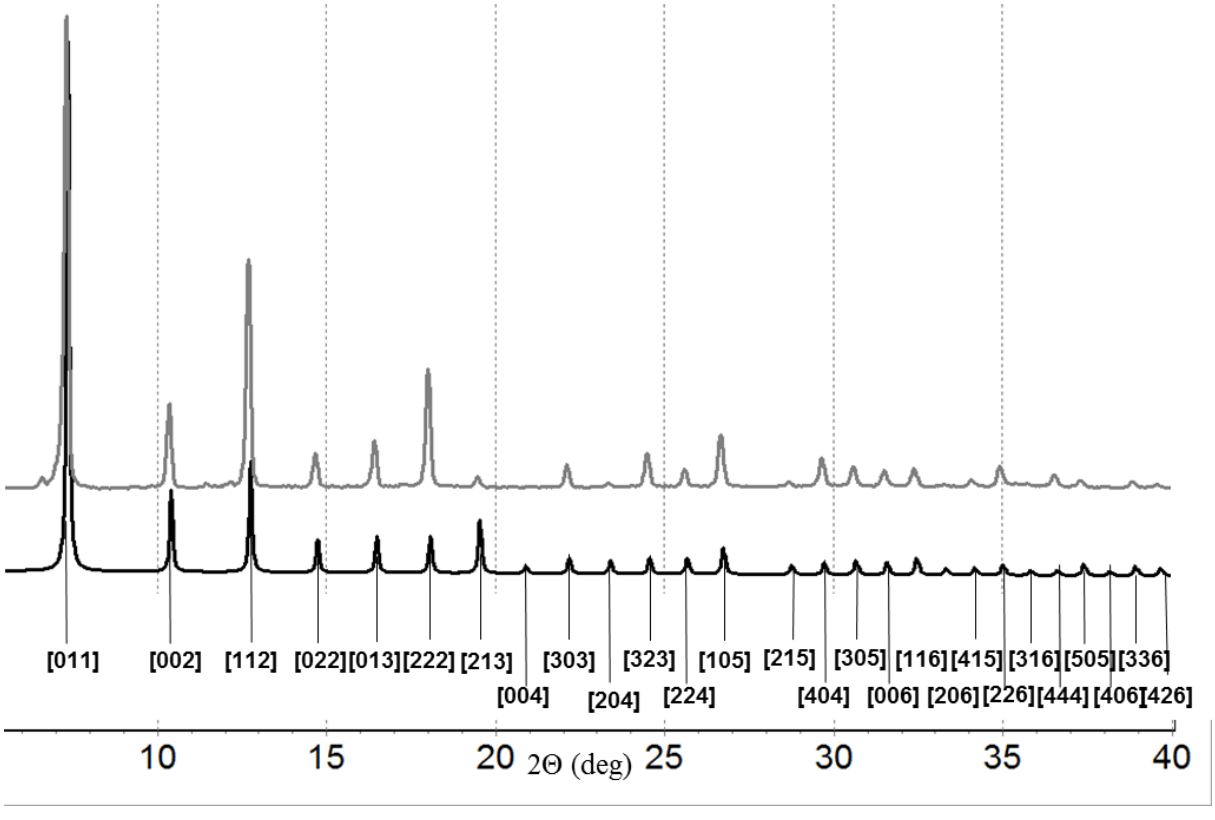

Figure S1. Powder XRD patterns of ZIF-8 produced hydrothermally with 2.6 mol of TEA (gray) and that calculated according to data from [5](black).

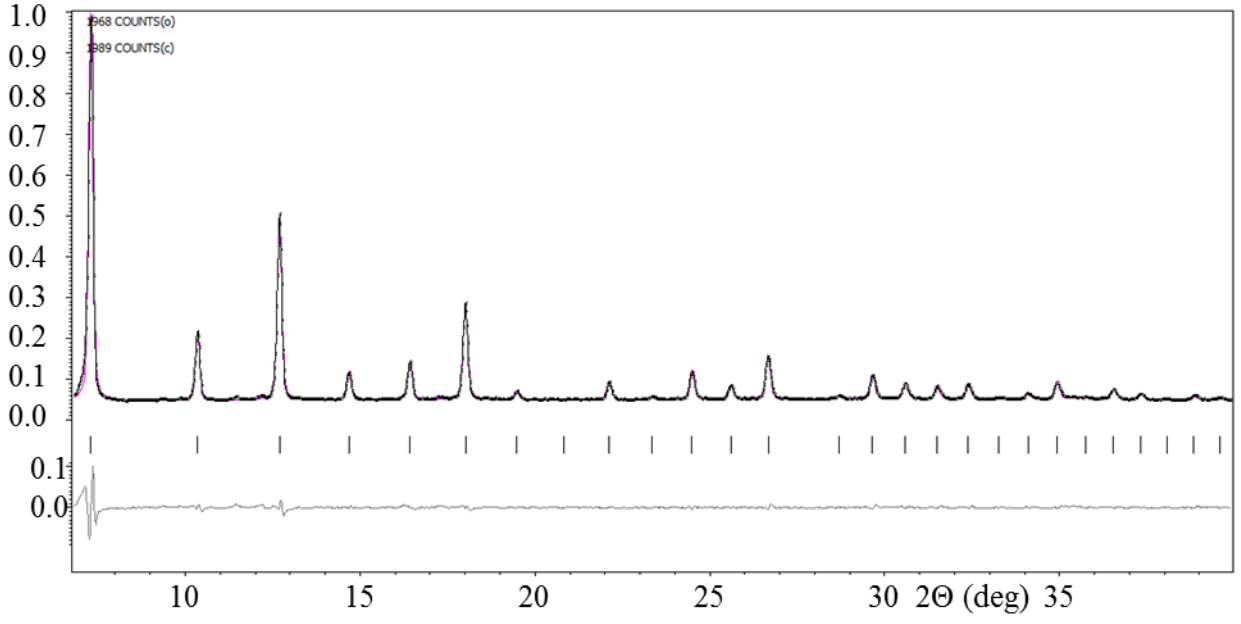

Figure S1. Powder XRD patterns of ZIF-8 produced hydrothermally and measured at room temperature: observed (black), calculated (red, almost completely overshadowed by the experimental curve), and their difference (gray). The short vertical bars indicate the Bragg positions of the reflections (obtained using Jana2006 program package).

3. Structure of the samples with low TEA content or without it.

Samples obtained with 1.9 or without of TEA had the same structure different from the SOD ZIF-8 structure. The same profile was previously reported by Bao et al. [16] for the sample obtained in water under MW heating with Hmim:Zn^{2+} ratio 2:1. However, this phase was not identified in [16]. We indexed structure in triclinic crystal system (Figure S3). TEM images revealed layered structure of this phase unlike well-shaped rhombic dodecahedron ZIF-8 crystals (see Figure 3 in main text).

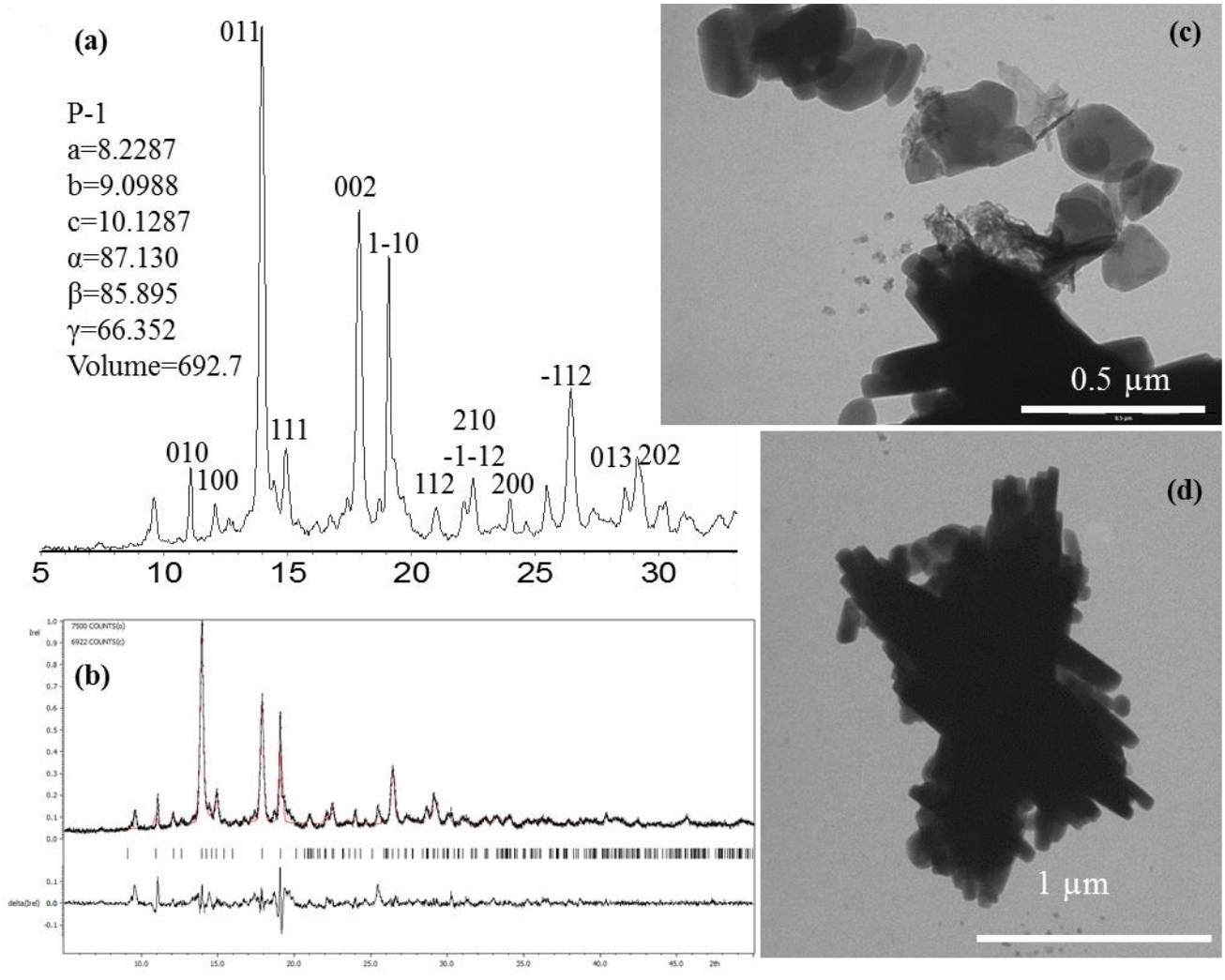

Figure S3. Part (a) demonstrates XRD profiles of sample, obtained without TEA, with indexes under reflections and structural information. (b) XRD patterns of the same sample: calculated (red), observed (black) and their difference (gray). The short vertical bars indicate the Bragg positions of the reflections (obtained using Jana2006 program package). (c) and (d) – TEM images of this sample.

TGA analysis of the phases with 1.9 TEA or without it revealed different from the ZIF-8 samples shape of the curves. Nitrogen adsorption isotherms are typical for non-porous materials (Figure S4). SSA of the sample, obtained without TEA is 10.8 m^2/g (BET). The Type H3 loop is typical for aggregates of plate-like particles giving rise to slit-shaped pores [18] in good agreement with TEM images.

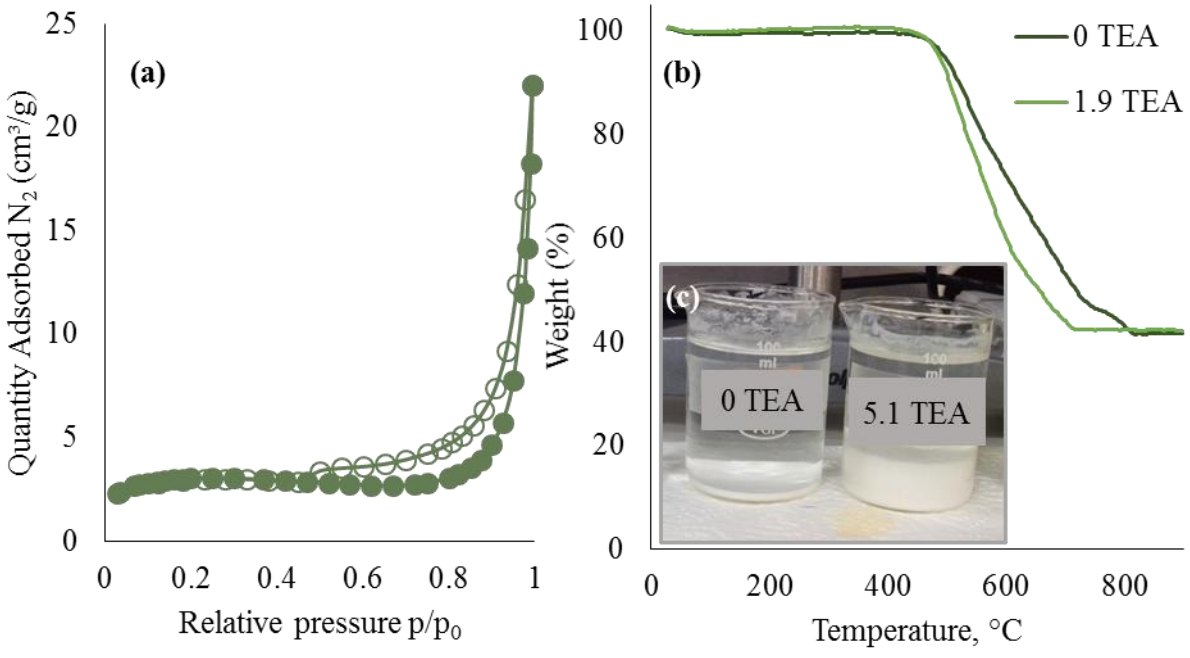

Figure S4. (a) Nitrogen adsorption isotherm of sample, obtained without TEA. (b) TGA curves for samples with 1.9 TEA(light green) and without it (dark green). (c) Photo of obtained samples. Left one – non-porous sample without of TEA and right one – ZIF-8 sample with 5.1 TEA.

4. XRD profiles of ZIF-8 sample treated in acidic and basic media and with iodine solution

For all stability tests, we used ZIF-8 sample, obtained with 2.6 mol TEA. Water, acidic and basic treatments were carried out under the ambient conditions. 0.1 g of ZIF-8 sample was dispersed in 10 ml of DI water, 0.1 M solutions of HCl or NaOH respectively. After that, suspension was stirred for 24 h. In acidic media sample was completely dissolved. Other two samples were centrifuged and dried at 80 °C in the air before XRD. As it demonstrated on the Figure S4 crystal structure of ZIF-8 samples did not change after water and basic treatments.

For investigation of iodine sorption, we used 0.16 M ethanol solution of I_2. In 5 ml of this solution, 16 mg of ZIF-8 powder was added. Suspension was stirred for 35 minutes at room temperature, than centrifuged and separated solid and liquid parts. Solid one was dried in the air and used for XRD analysis. Optical spectra were measured from the liquid one.

The full sorption of iodine could be observed after centrifuge – orange solution became colorless and white powder became yellow (see photo in the figure S4). XRD measurement did not revealed any changes in the crystal structure of the sample, and optical spectra of the solution after treatment did not revealed any iodine.

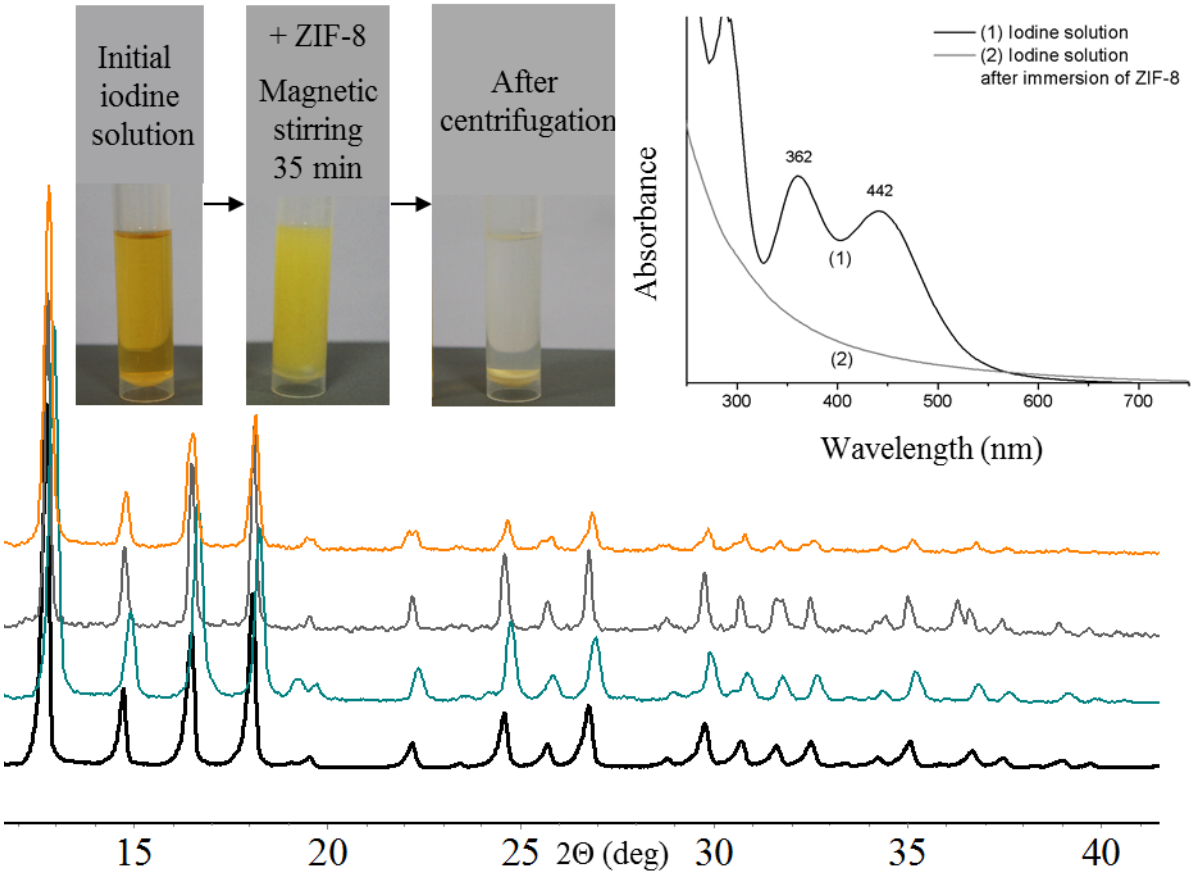

Figure S5. XRD profiles of samples ZIF-8 with 2.6 TEA. Black one - initial sample as is; blue - after water treatment; gray – after NaOH treatment, orange – after iodine adsorption.

5. TGA data

TGA curves for all samples with different TEA content were measured both in the air and in the nitrogen atmosphere. All samples demonstrate common tendency: in the air, decomposition of linker began at the lower temperature. The TEA content do not significantly changes shape of the curves, unlike the ambient atmosphere does.

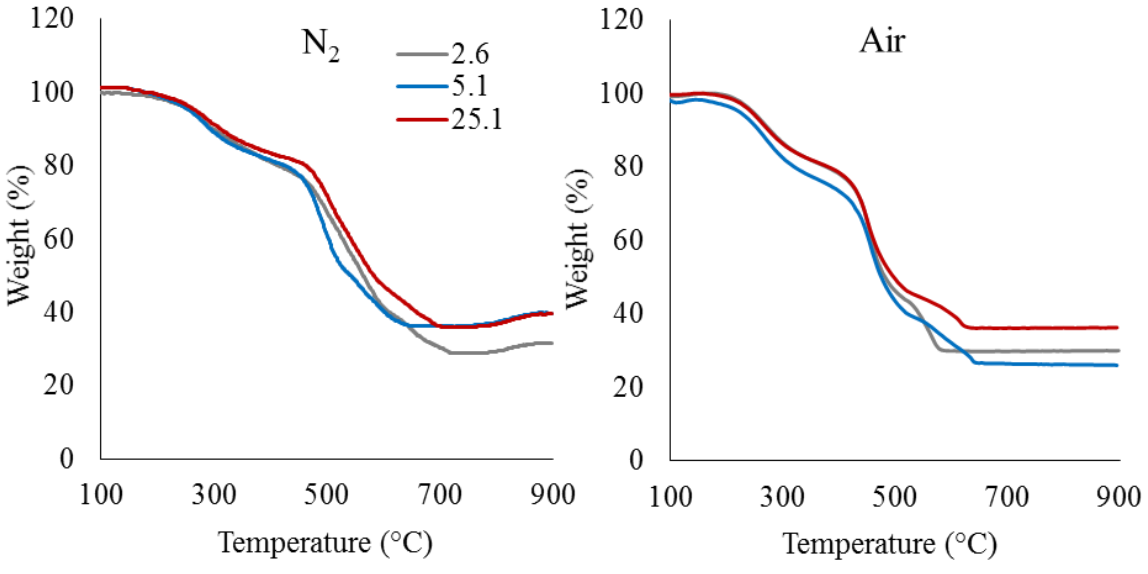

Figure S6. TGA curves for samples with different TEA content measured in the nitrogen (left) and in the air (right).

6. XRD profiles of ZIF-8 sample heated till 400 °C

Thermal stability of the sample was studied *in-situ* in Low-Temperature Chamber TTK 450 (Anton Paar) inside the ARL X'TRA. The sample in chamber was exposed to the step-by-step process of heating in 25-400 °C temperature range under continuous removal of generated solvent vapor. At each of the six steps, the measurement was performed after stabilization of the temperature.

The sequence of XRD patterns is shown in Fig. S7a with the curves shifted vertically for easy reading. The pattern at 450 °C was obtained in air, allowing formation of zinc oxide, whose yield by weight was 28 %. In order to better appreciate the changes in the structure of the sample caused by the increasing temperature, the development of three low-angle reflexes is given in Fig. S7b The data obtained (see Table S2) allows us to plot a dependence of unit cell parameter value versus the temperature (shown in Fig. S7c).
As can be seen from the thermo-diffractometry data, the structure of ZIF-8 is retained up to 400 °C. However, starting from 300 °C some noticeable degradation of crystallinity becomes evident. The unit cell parameter slightly increases at 200 and then decreases with the rise of temperature. The increment of the unit cell parameter can be attributed to the thermal expansion of the lattice, due to measuring XRD at elevated temperature. To prove it we have measured XRD of the sample, which was heated up to 200 °C and then was cooled own to room temperature. In this case, we observed slightly decreasing of unit cell parameters. Further reduction, although accompanied by shifting and widening of the reflexes (Fig. S7b), could relate to the partial decomposition of molecules of the linker leading to the changes in ZIF-8 phase and subsequent collapse of the MOF structure. It should be noted, that under the vacuum or in the nitrogen atmosphere samples are more stable and preserve their structure up to 430 °C.

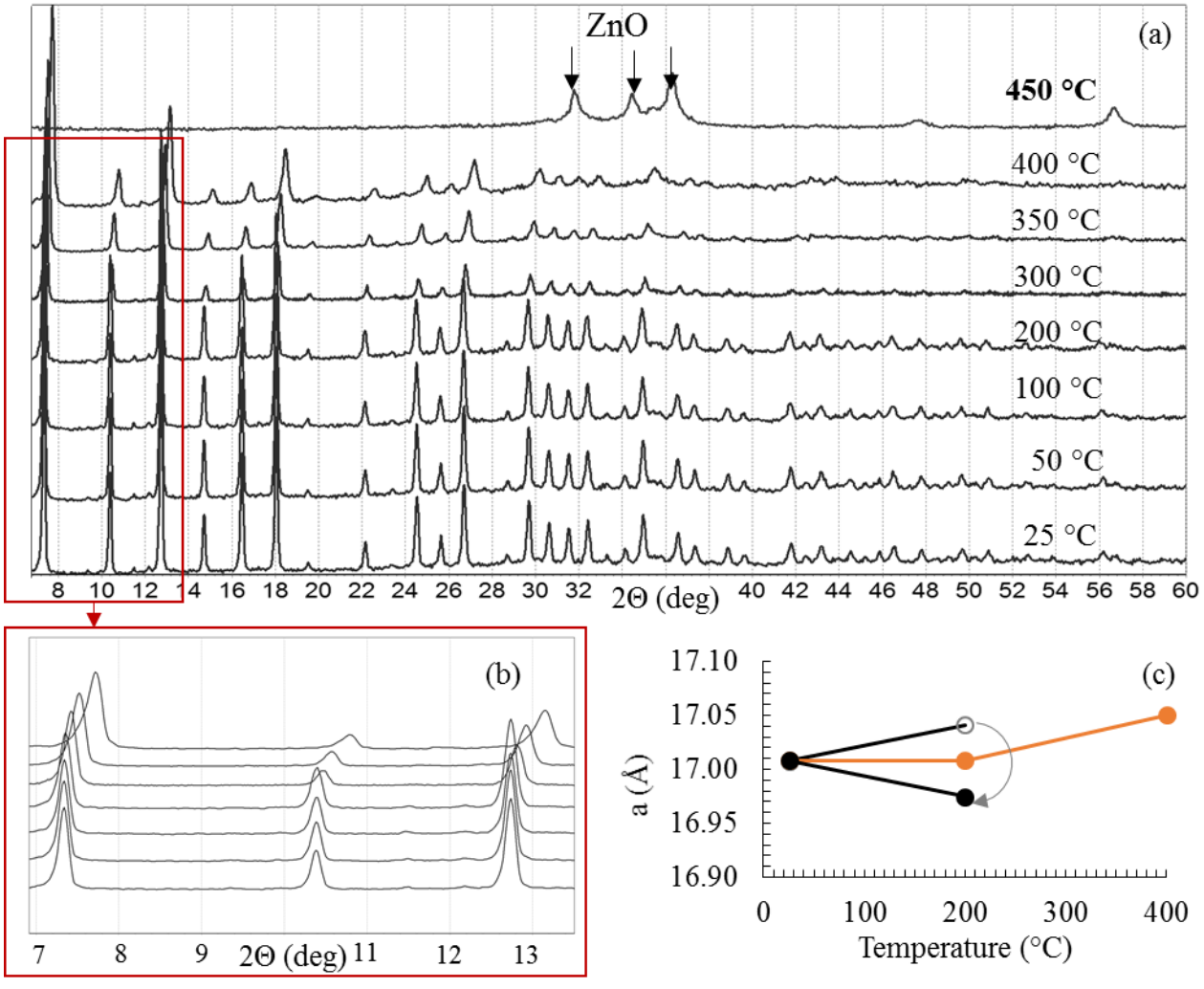

Figure S7. Study of the thermal stability of ZIF-8 by powder XRD: (a) diffraction patterns recorded in 25-400 °C temperature range for sample under continuous removal of generated solvent vapor; sample at 450 °C was annealed in the air; (b) shift and widening of the reflexes shown in 2Θ range from 7 to 13 ° for patterns in a); (c) changes of unit cell parameter a value during heating of the sample. Black open marker correspondes a value of the hot sample, filled marker – of the sample, which was cooled down. Orange plot is attributed to the sample heated under the vacuum.

Table S2. Details of XRD profile analysis for ZIF-8 samples at different temperatures.

Temperature, °C	*a*, Å	GOF (χ^2), %	R_p, %	wR_p, %
25	16.9986(7)	2.30	6.90	9.15
50	17.0069(7)	2.31	6.94	9.16
100	17.0205(7)	2.27	6.78	8.93
200	17.0413(8)	2.29	6.81	8.94
300	16.9990(11)	2.47	7.11	9.60
350	16.9612(15)	2.35	6.97	9.41
400	16.909(3)	2.37	7.71	10.25

7. Detailed analyses of adsorption isotherms

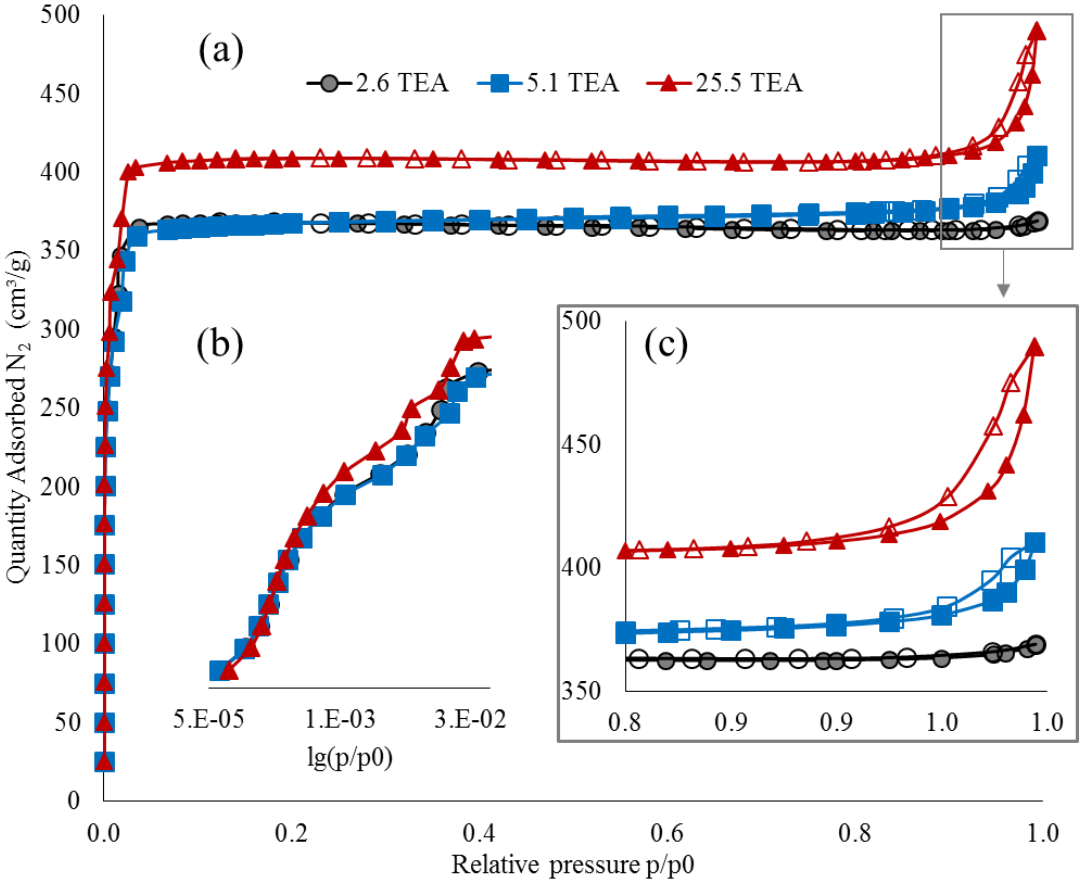

Figure S8. (a) Isotherms of nitrogen physisorption at 77 K on ZIF-8 with different quantity of added TEA. The adsorption branch is shown by filled markers and the desorption one by open markers. (b) The same isotherms in a logarithmic-scale plot. (c) Part of isotherms with hysteresis loops magnified for clarity.

The part (b) in Fig. S8 shows the isotherm, plotted in semi-logarithmic scale to better analyze the range of lower pressures. In particular, one can see a double step rise: first at $p/p_0 = 7.89 \cdot 10^{-4}$, second at $p/p_0 = 1.869 \cdot 10^{-2}$. The two-step uptake was already observed in the ZIF-8 obtained in different ways, and are attributed to the structural reorganization of the adsorbate molecules in the micropores of the MOF when reaching certain threshold pressures (with some similarities to zeolites) [5]. This effect is particularly pronounced in the case of ZIF-8 material due to close size of the windows to the pores (3.4 Å) and size of nitrogen molecule (3.64 Å). The other explanation was given in [19] and considered with reversible transformation in the structure of ZIF-8 phase after reaching the step pressure value, which leads to the increase of windows to the pores.

There is a clear trend of increase in uptake over $p/p_0 > 0.9$ along with rising quantity of TEA. This effect is thought to be related to filling the pores (mesopores) between adjacent nanocrystals of sample [20], textural meso/macroporosity fromed by packing of NPs [11] and higher interparticle porosity [17]. Above $p/p_0 = 0.8$ a weak hysteresis of H1 type is observed, which may indicate the presence of narrow slit-like micropores in the material [18]. We suppose that this kind of pores are formed between particles in aggregates. The loop became more pronounced with increase of TEA content in agreement with decreasing of particle size.

8. TEM images

All samples was prepeared by ultrasaund treatment in isopropanoll for 30 minutes in order to separate particles. Few drops of obtained suspension was placed into the carbon-coated copper grids. For each sample was done number of images. Particle size was estimated by means of an image analysing program (Digimizer).

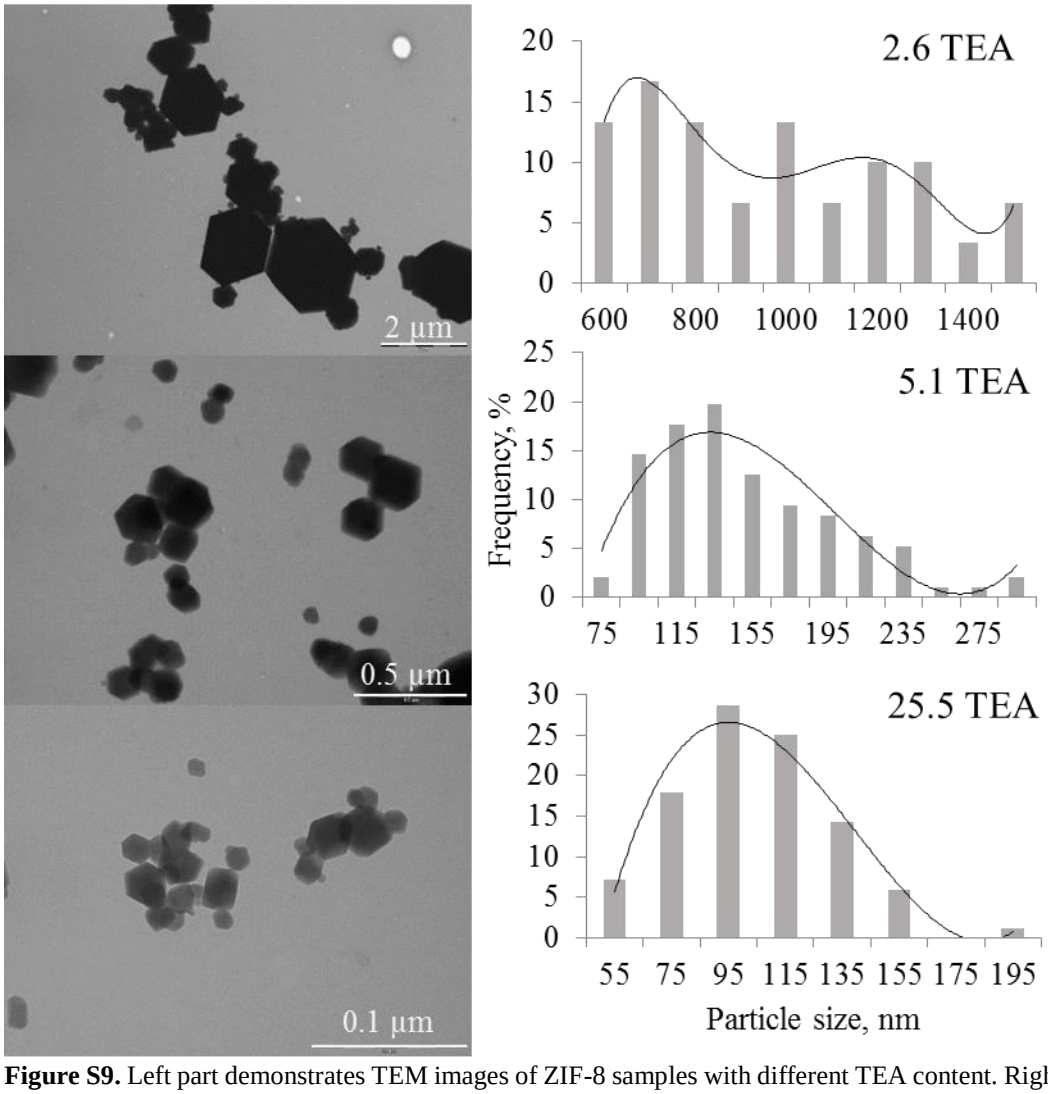

Figure S9. Left part demonstrates TEM images of ZIF-8 samples with different TEA content. Right part – particle size distribution of the appropriate sample.

9. FTIR spectroscopy

FTIR spectroscopy using the potassium bromide pelleting technique was performed to obtain some reference data on the same instrument to be then compared with measurement results collected on the synthesized samples. Fig. S8 allows to confront the curves of KBr itself, two precursors of ZIF-8, namely, zinc nitrate and 2-methylimidazole, ZIF-8 produced commercially by BASF under Basolite Z1200 name, and, finally, synthetized by us ZIF-8 with use of 2.6 mol of TEA. Additionally, characteristic reference IR data for ZIF-8 published by Park *et al.*, 2006 (see the main text for reference details) is given by bars, whose height reflects the intensity coding for IR-bands: weak, medium and strong.

The IR profile of KBr contains contributions from physisorbed water (3500-3300 and 1630 cm^{-1}) and from potassium carbonate (1380 and 873 cm^{-1}) formed on its surface under open-air conditions. The IR spectrum of zinc nitrate contains dominating bands () of nitrate anion and low-intensity bands due to overtones as well as those present on KBr. The 2-Hmim curve exhibits complex vibrational picture and will be commented briefly. It has a broad group of strong peaks at high-frequency end of spectrum (3000-2500 cm^{-1}) originating from hydrogen bonding between the pyrrole group and the pyridinic nitrogen (N–H ⋯ N). Slightly above 3000 cm^{-1} appear the aliphatic C–H stretching. The bands at 1596 and 731 cm^{-1} are due to C–N stretching and bending vibrations, while that at 600 cm^{-1} originates from C=N stretching. The bands about 1450 cm^{-1} relate to ring stretching, while some of those at lower frequencies stand for C–H bending and other come from the ring distortion modes. Disappearance of the (N–H ⋯ N) bending and the N–H stretching vibrations in ZIF-8 spectra suggest that Hmim linkers are fully deprotonated.

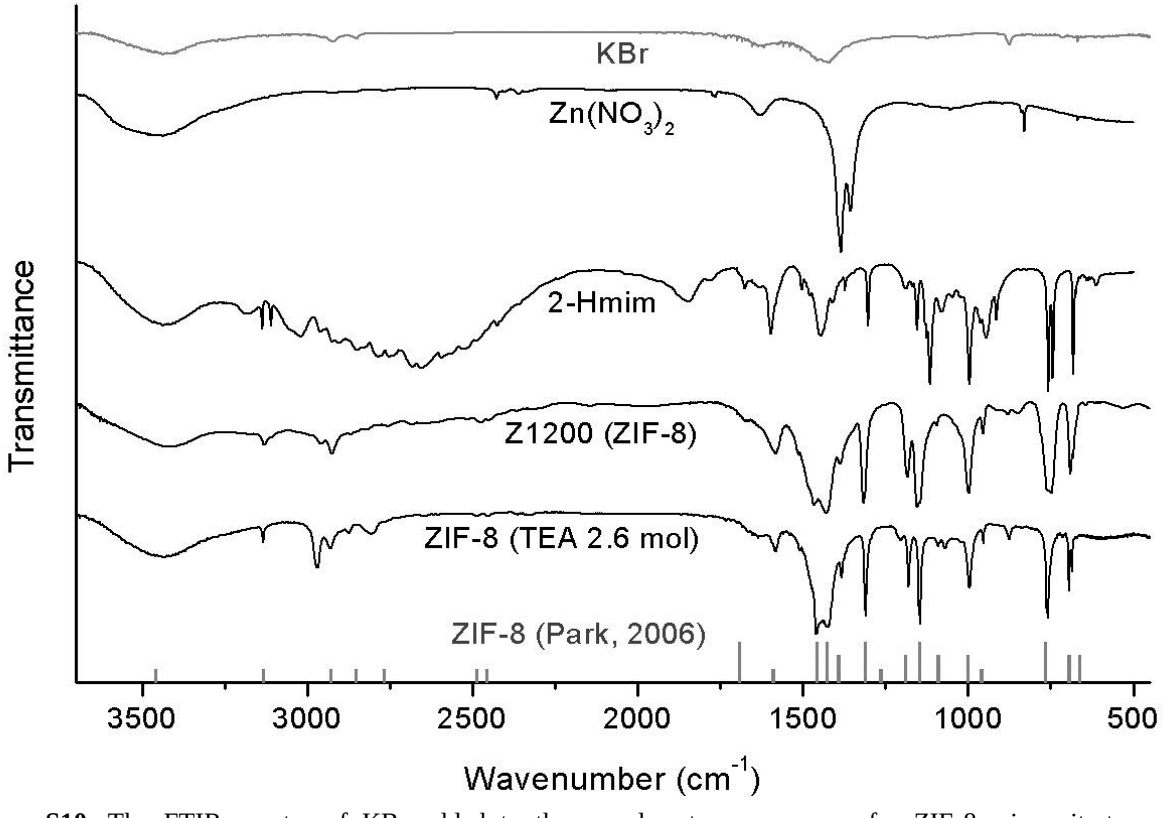

Figure S10. The FTIR spectra of KBr added to the samples, two precursors for ZIF-8: zinc nitrate and 2-methylimidazole, Z1200, a commercial version of ZIF8 (BASF), and ZIF-8 (TEA 2.6 mol) obtained in this work. The spectra are shifted vertically for clarity. Bars mark the positions of characteristic IR-bands (of weak, medium and strong intensity) for ZIF-8 reported in the work of Park et al., 2006 (see the main text for reference details).

In order to appreciate in more details the "fingerprint" region of the Mid-IR spectra, the FTIR spectra of extended sequence of the samples (including ZIF-8 obtained with TEA content of 2.0 and 3.0 mol and not reported in Fig. 3 of the main text for sake of clarity) are reported in Fig. S9 (being vertically shifted for clarity). Above all the reference spectrum of KBr used for preparation of pellets (discs) is shown.

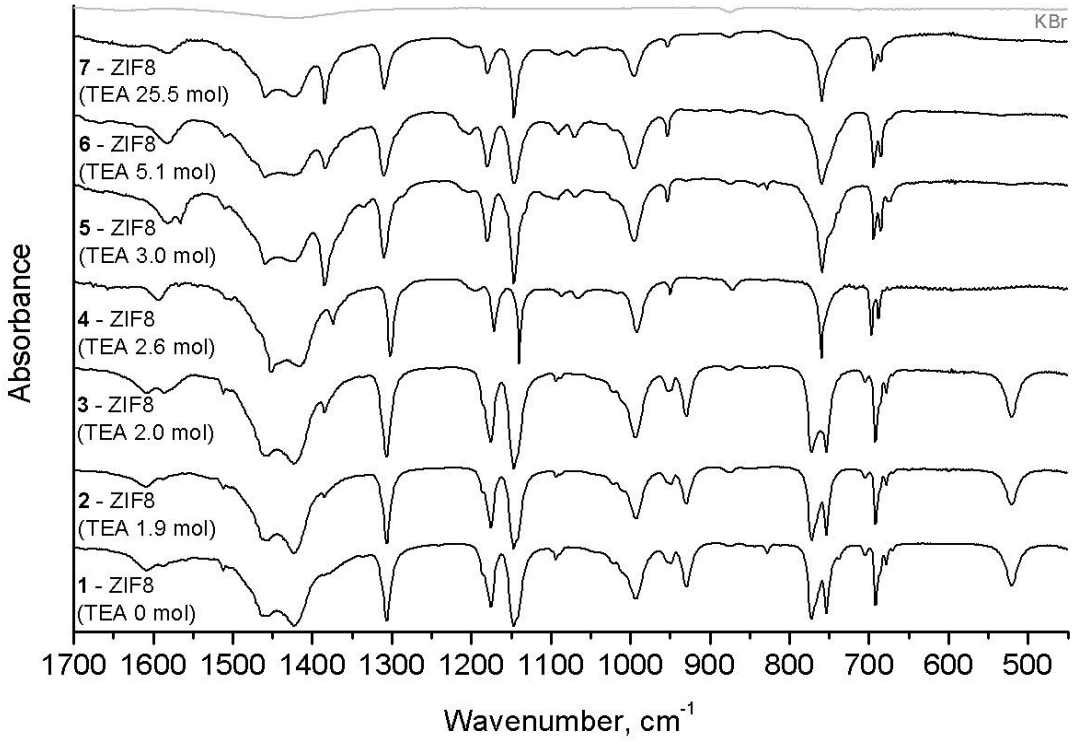

Figure S11. The FTIR spectra of ZIF8 samples obtained with different amount of TEA.

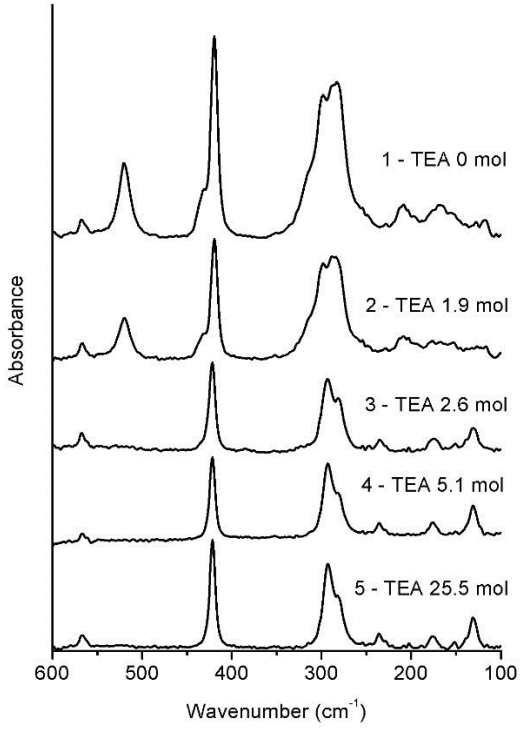

Figure S12. The ATR-FTIR spectra of ZIF8 samples obtained with different amount of TEA.

10. Analysis of chemical reactions during adopted synthesis of ZIF-8

10.1. Calculations proving the formation of $Zn(OH)_2$ precipitate in case of adding TEA to the zinc precursor salt

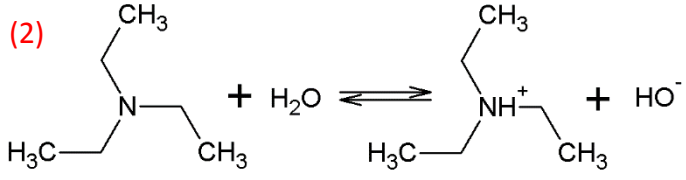

(2) $(C_2H_5)_3N + H_2O = (C_2H_5)_3NH^+ + OH^-$, K_2

(5) $Zn^{2+} + 2OH^- = Zn(OH)_2$

$$K_2 = \frac{[(C_2H_5)_3NH^+]\cdot[OH^-]}{[(C_2H_5)_3N]} = \frac{[(C_2H_5)_3NH^+]\cdot[OH^-]}{[(C_2H_5)_3N]} \cdot \frac{[H^+]}{[H^+]} = \frac{Kw}{k_a(TEA)} = \frac{10^{-14}}{1.65\cdot10^{-11}} = 6\cdot10^{-4}$$

$Kw = [H^+]\cdot[OH^-]=10^{-14}$

$[OH^-] = [(C_2H_5)_3NH^+] = x$; $[(C_2H_5)_3N] = C((C_2H_5)_3N)_{initial} - x$

$$K_2 = \frac{x^2}{C((C_2H_5)_3N)-x} = \frac{x^2}{0.233-x} = 6\cdot10^{-4}$$

$X = 0.012 = [OH^-]$

The equilibrium concentrations of the compounds are given in square brackets. All used dissociation constants was from [21].

Concentration of OH^- groups in 25 ml TEA solution is 0.012 mol/l and Zn^{2+} concentration in the same solution – 0.0896 mol/l. So the ionic product of these ions ($1.25\cdot10^{-5}$) is bigger than solubility of $Zn(OH)_2$ (10^{-17}). Therefore, a precipitate will be obtained.

10.2. Calculation of equilibrium constants and pH values

(1) Hydrolysis of linker in water solution without of TEA

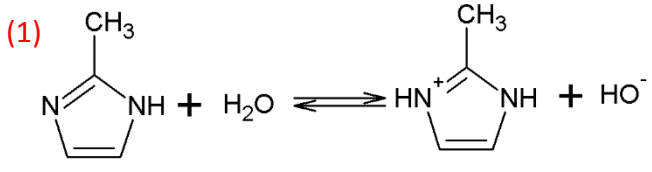

(1) $Hmim + H_2O \leftrightarrow H_2mim^+ + OH^-$, **$k_1$**

(1.1) $H_2mim^+ \leftrightarrow Hmim + H^+$, $k_{BH^+}=10^{-7.85}$, [13]

(1.2) Hmim ↔ mim^- + H^+, $k_a=10^{-15.1}$, [13]

$$k_1 = \frac{[H_2mim^+]\cdot[OH^-]}{[Hmim]} = \frac{[H_2mim^+]\cdot[OH^-]}{[Hmim]}\cdot\frac{[H^+]}{[H^+]} = \frac{kw}{k_{BH^+}} = \frac{10^{-14}}{10^{-7.85}} = \mathbf{7.08\cdot10^{-7}}$$

$[OH^-] = [H_2mim^+] = y$; $[Hmim] = C(Hmim)_{initial}-y$

$$k_1 = \frac{y^2}{C(Hmim)-y} = \frac{y^2}{0.3585-y} = \mathbf{7.08\cdot10^{-7}}$$

$$y = 5\cdot10^{-4} = [OH^-]$$

$$[H^+] = \frac{kw}{[OH^-]} = \frac{10^{-14}}{5\cdot10^{-4}} = 2\cdot10^{-11}$$

$pH = -\log[H^+]$

pH =10.7

10.3. Overall equilibrium of Hmim reaction with TEA in water medium

We suggest three possible reaction routs in 3-component system of Hmim-TEA-H_2O. In order to choose one process, we have calculated equilibrium constants.

(3)

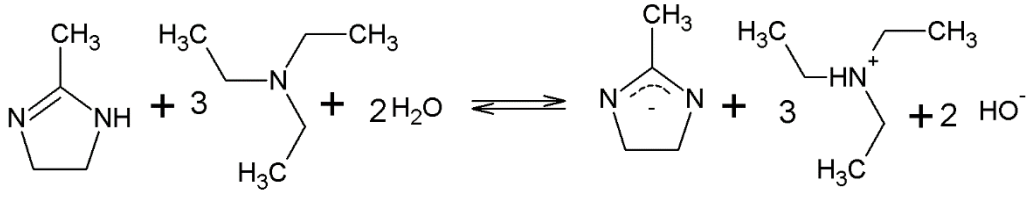

Hmim + H_2O + $2(C_2H_5)_3N$ + H_2mim^+ + $(C_2H_5)_3N$ + H_2O ↔ H_2mim^+ + OH^- + mim^- + $2(C_2H_5)_3NH^+$ + $(C_2H_5)_3NH^+$ + OH^-

(3) Hmim + $3(C_2H_5)_3N$ + $2H_2O$ ↔ mim^- + $3(C_2H_5)_3NH^+$ + $2OH^-$, k_3

$$k_3 = \frac{[mim^-]\cdot[(C_2H_5)_3NH^+]^3\cdot[OH^-]^2}{[(C_2H_5)_3N]^3\cdot[Hmim]} = \frac{[mim^-]\cdot[(C_2H_5)_3NH^+]^3\cdot[OH^-]^2}{[(C_2H_5)_3N]^3\cdot[Hmim]}\cdot\frac{[H^+]}{[H^+]}$$

$$= k_a\cdot\frac{[(C_2H_5)_3NH^+]^3\cdot[OH^-]^2}{[(C_2H_5)_3N]^3\cdot[H^+]} = k_a\cdot\frac{[(C_2H_5)_3NH^+]^3\cdot[OH^-]^2}{[(C_2H_5)_3N]^3\cdot[H^+]}\cdot\frac{[OH^-]}{[OH^-]}$$

$$= \frac{k_a\cdot{k_2}^3}{[H^+]\cdot[OH^-]} = \frac{k_a\cdot{k_2}^3}{kw}$$

$$k_3 = \frac{10^{-15.1}\cdot(6\cdot10^{-4})^3}{10^{-14}} = \mathbf{1.72\cdot10^{-11}}$$

(4)

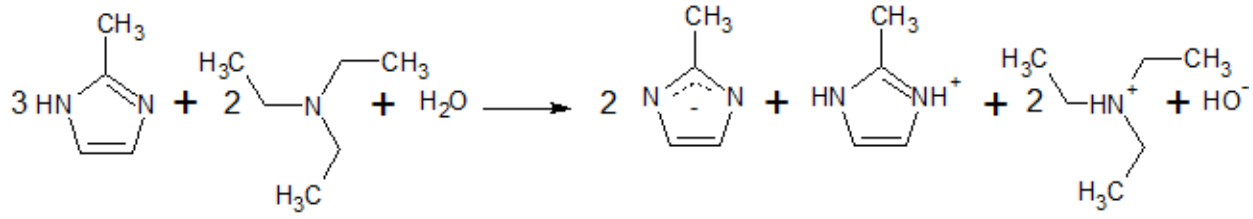

(4) $3Hmim + 2(C_2H_5)_3N + H_2O \leftrightarrow 2mim^- + 2(C_2H_5)_3NH^+ + OH^-$, k_4

$$k_4 = \frac{[mim^-]^2 \cdot [H_2mim^+] \cdot [(C_2H_5)_3NH^+]^2 \cdot [OH^-]}{[(C_2H_5)_3N]^2 \cdot [Hmim]^3} =$$

$$= \frac{[mim^-]^2 \cdot [H_2mim^+] \cdot [(C_2H_5)_3NH^+]^2 \cdot [OH^-]}{[(C_2H_5)_3N]^2 \cdot [Hmim]^3} \cdot \frac{[H^+]^3}{[H^+]^3}$$

$$= \frac{[mim^-]^2 \cdot [H^+]^2}{[Hmim]^2} \cdot \frac{[H_2mim^+]}{[Hmim] \cdot [H^+]} \cdot \frac{[(C_2H_5)_3NH^+]^2}{[(C_2H_5)_3N]^2 \cdot [H^+]^2} \cdot [H^+] \cdot [OH^-] =$$

$$= k_a(Hmim)^2 \cdot \frac{1}{k_{BH+}} \cdot \frac{1}{k_a(TEA)^2} \cdot kw$$

$$k_4 = \frac{(10^{-15.1})^2 \cdot 10^{-14}}{10^{-7.85} \cdot (1.65 \cdot 10^{-11})^2} = \mathbf{1.64 \cdot 10^{-15}}$$

(5)

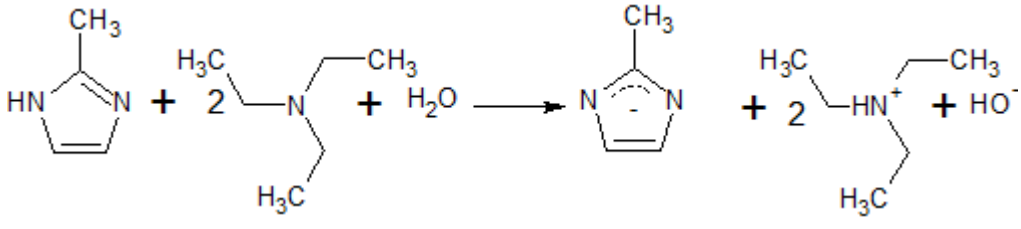

(5) $Hmim + 2(C_2H_5)_3N + H_2O \leftrightarrow mim^- + 2(C_2H_5)_3NH^+ + OH^-$, k_5

$$k_5 = \frac{[mim^-] \cdot [(C_2H_5)_3NH^+]^2 \cdot [OH^-]}{[(C_2H_5)_3N]^2 \cdot [Hmim]} = \frac{[mim^-] \cdot [(C_2H_5)_3NH^+]^2 \cdot [OH^-]}{[(C_2H_5)_3N]^2 \cdot [Hmim]} \cdot \frac{[H^+]^2}{[H^+]^2} =$$

$$= \frac{[mim^-] \cdot [H^+]}{[Hmim]} \cdot \frac{[(C_2H_5)_3NH^+]^2}{[(C_2H_5)_3N]^2 \cdot [H^+]^2} \cdot [H^+] \cdot [OH^-] =$$

$$= k_a(Hmim) \cdot \frac{1}{k_a(TEA)^2} \cdot kw$$

$$k_5 = \frac{10^{-15.1} \cdot 10^{-14}}{(1.65 \cdot 10^{-11})^2} = \mathbf{2.918 \cdot 10^{-8}}$$

As $k_5 > k_3 > k_4$ we suppose that this process will dominate in the reaction mixture. Therefore, we used this value to calculate pH.

$[mim^-] = z$; $[OH^-] = z$; $[(C_2H_5)_3NH^+] = 2z$

$[Hmim] = C(Hmim)_{initial} - z$

$[(C_2H_5)_3N] = C((C_2H_5)_3N)_{initial} - 2z$

$$k_5 = \frac{z \cdot (2z)^2 \cdot z}{(C(Hmim)_{initial} - z) \cdot (C((C_2H_5)_3N)_{initial} - 2z)^2} = \mathbf{2.918 \cdot 10^{-8}}$$

$$k_5 = \frac{4z^4}{(0.3385 - z) \cdot (C((C_2H_5)_3N)_{initial} - 2z)^2} = \mathbf{2.918 \cdot 10^{-8}}$$

Table S2. *The calculation results of pH values for various TEA concentrations.*

n (TEA) in respect to 1 mol of Zn^{2+}	$C((C_2H_5)_3N)_{initial}$	$[OH^-]=z$	$[H^+]=k_w/[OH^-]$	pH
1.9	0.1703	0.0029	$3.50 \cdot 10^{-12}$	11.46
2.6	0.2330	0.0034	$2.95 \cdot 10^{-12}$	11.53
5.1	0.4571	0.0048	$2.10 \cdot 10^{-12}$	11.67
25.5	2.2853	0.0107	$9.36 \cdot 10^{-12}$	12.02

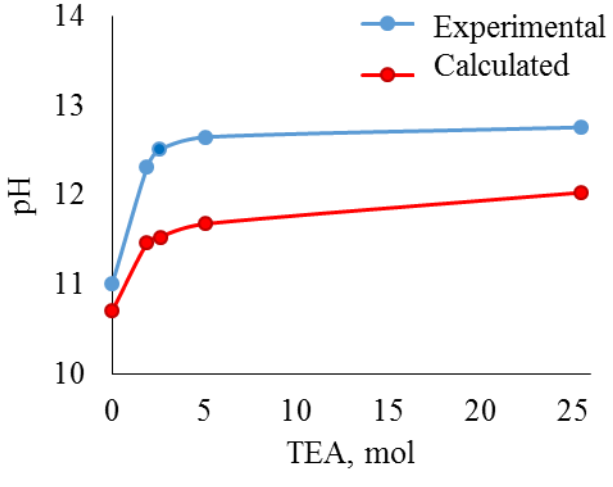

Figure S13. Increase of pH upon addition of TEA to Hmim solution. TEA quantity is given in respect to 1mol of Zn^{2+}. Blue line represents measured pH values, red one – theoretically calculated.

As it follows from the Figure S13 trend in pH increasing obtained both from experimental and calculated data is the same. After 5 mol of TEA we observed a plateau, so further increase of TEA concentration did not resulted in any significant increase of pH values. However, calculated values of pH are lower than measured ones. It could be attributed to some secondary process in the reaction mixture, which were neglected in our calculations. However, as calculated pH values are rather

similar to the experimental one and the trend in their changes predicted correctly, we suppose that proposed reaction schemes and equilibrium constants could be useful for further investigations.

REFERENCES for Supporting Information

[1] X.-C. Huang, Y.-Y. Lin, J.-P. Zhang, X.-M. Chen, Angew. Chem. Int. Ed., 45 (2006) 1557-1559.
[2] C. Chizallet, S. Lazare, D. Bazer-Bachi, F. Bonnier, V. Lecocq, E. Soyer, A.-A. Quoineaud, N. Bats, J. Am. Chem. Soc., 132 (2010) 12365-12377.
[3] H. Bux, F. Liang, Y. Li, J. Cravillon, M. Wiebcke, J. Caro, J. Am. Chem. Soc., 131 (2009) 16000-16001.
[4] J. Cravillon, R. Nayuk, S. Springer, A. Feldhoff, K. Huber, M. Wiebcke, Chem. Mater., 23 (2011) 2130-2141.
[5] K.S. Park, Z. Ni, A.P. Côté, J.Y. Choi, R. Huang, F.J. Uribe-Romo, H.K. Chae, M. O'Keeffe, O.M. Yaghi, Proceedings of the National Academy of Sciences, 103 (2006) 10186-10191.
[6] H.-L. Jiang, B. Liu, T. Akita, M. Haruta, H. Sakurai, Q. Xu, J. Am. Chem. Soc., 131 (2009) 11302-11303.
[7] U.P.N. Tran, K.K.A. Le, N.T.S. Phan, ACS Catalysis, 1 (2011) 120-127.
[8] S. Liu, Z. Xiang, Z. Hu, X. Zheng, D. Cao, J. Mater. Chem., 21 (2011) 6649-6653.
[9] X. Fan, W. Wang, W. Li, J. Zhou, B. Wang, J. Zheng, X. Li, ACS Applied Materials & Interfaces, 6 (2014) 14994-14999.
[10] V.V. Butova, A.P. Budnik, E.A. Bulanova, A.V. Soldatov, Mendeleev Commun., 26 (2016) 43-44.
[11] Y. Pan, Y. Liu, G. Zeng, L. Zhao, Z. Lai, Chem. Commun., 47 (2011) 2071-2073.
[12] A.F. Gross, E. Sherman, J.J. Vajo, Dalton Transactions, 41 (2012) 5458-5460.
[13] K. Kida, M. Okita, K. Fujita, S. Tanaka, Y. Miyake, CrystEngComm, 15 (2013) 1794-1801.
[14] N.A.H.M. Nordin, A.F. Ismail, A. Mustafa, P.S. Goh, D. Rana, T. Matsuura, RSC Advances, 4 (2014) 33292-33300.
[15] Q. Shi, Z. Chen, Z. Song, J. Li, J. Dong, Angew. Chem. Int. Ed., 50 (2011) 672-675.
[16] Q. Bao, Y. Lou, T. Xing, J. Chen, Inorg. Chem. Commun., 37 (2013) 170-173.
[17] M. Jian, B. Liu, R. Liu, J. Qu, H. Wang, X. Zhang, RSC Advances, 5 (2015) 48433-48441.
[18] K.S.W. Sing, D.H. Everett, R.A.W. Haul, L. Moscou, R.A. Pierotti, J. Rouquerol, T. Siemieniewska, Pure Appl. Chem., 57 (1985) 603-619.
[19] D. Fairen-Jimenez, S.A. Moggach, M.T. Wharmby, P.A. Wright, S. Parsons, T. Düren, J. Am. Chem. Soc., 133 (2011) 8900-8902.
[20] J. Cravillon, S. Münzer, S.-J. Lohmeier, A. Feldhoff, K. Huber, M. Wiebcke, Chem. Mater., 21 (2009) 1410-1412.
[21] D.D. Perrin, Dissociation Constants of Organic Bases in Aqueous Solution Butterworths, 1972.